ALMA MATER STUDIORUM
UNIVERSITY OF BOLOGNA

School of Engineering

Master Degree in Automation Engineering

Master Thesis

Electroactive soft actuators: modelling and control

CANDIDATE:
Giovanni Paoletta

SUPERVISORS:
Gianluca Palli,
Raffaella Carloni

CO-SUPERVISOR:
Riccardo D'Anniballe

Academic year 2018/2019

Graduation Session III

A zio Tonino

"È uscito il sole"

“ La natura universale questo fa: sposta le cose, le trasforma, le prende da una parte e le porta da un’altra. Tutto è mutamento, ma ogni cosa è distribuita in modo armonico ed equilibrato, sicché nulla d’insolito può accadere che non rientri in quest’ordine, e nulla dobbiamo temere di nuovo.”

Marco Aurelio, A sé stesso, VIII, 6; 2008

Abstract

The work done in this master thesis is part of the European project MAGNIFY[1] at the University of Groningen, the Netherlands."MAGNIFY aims to develop a new generation of artificial muscles for robotic systems. The artificial muscle will be realized by using artificial molecular machines, organized in polymer nanofibers and individually controlled by external stimuli" [2]. This thesis focuses on a similar polymer that will be used in the project MAGNIFY. The work presents the analysis and utilization of an electroactive soft actuator, made of polyurethane-based nanofibers. A mat of aligned nanofibers of polyurethane and salt has been fabricated through an electrospinning process and, subsequently, has been rolled up to form a bundle of aligned nanofibers. Several electromechanical tests have been performed on the bundle, applying a certain voltage and evaluating the force and the displacement generated by the soft actuator. The sampled data of voltage, force, and displacement are then used to identify the nonlinear model of *Voltage-Force* and *Voltage-Displacement* link. The second part of this thesis aims to use the model estimated *Voltage-Displacement* to build a PID controller for position control. It has been shown a possible future application for the soft actuator as a robotic arm. To conclude, an energy analysis has been performed, to compare the energy consumption of the soft-actuator and of an electric linear motor, considering similar maximum output force.

[1]This project has received funding from the European Union's Horizon 2020 Research and Innovation Programme under Grant Agreement no. 801378.

[2]https://www.magnifyproject.eu/project-overview

Contents

List of Figures

Introduction

Motivation

Polyurethane (PU) is a versatile thermoplastic polymer. PU has a good mechanical property such as flexibility and low density. The PU is also bio-compatible and is biodegradable, so is easily suitable for medical materials, for example for drug delivery [3].

Polyurethane has been used as a soft actuator. In [9] the bending characteristics of a polyurethane elastomer film with different metal electrodes have been analyzed; Iron chloride has been electrospun with a polyurethane matrix in [12] to realize a conductive nanofibrous actuator, while in [1] carbon powders have been used as conductive filler in a polyurethane film to realize MEMS actuators. As pointed out, for example, in [11], controlling soft robots requires new approaches to modelling, control, dynamics, and high-level planning. Known robotics techniques for kinematic and dynamic modelling cannot be directly used in soft robotics; soft robots are highly nonlinear systems and the sensitivity of the materials can easily cause a change in the dynamics of the system. Several approaches can be found in literature to realize a control model for soft robots: in [15] or in [6] a FEM methodology is used to get a dynamical model of the soft robots, in [16] six different control approaches inspired by classical control theory, machine learning, and neuroscience were evaluated in controlling a cable-driven robot. The nonlinear system identification theory, proposed in this work, could be useful when the physics of the system is too complex to be described just by physical insight; black-box modelling is a good approach for soft robotics, where the different physical effect is the reason of movement of actuators. This paper focuses on a soft actuator realized as a bundle of aligned nanofibers of polyurethane and salt that acts as conductive filling, lowering the electrical resistance of the material. In fact, the driving characteristics of the actuator are influenced by phenomena related to the flowing of current in the material [12]. The nanofibers have been realized through the electrospinning process. Electrospinning is an efficient technique to produce small-diameter (from nanometer to micrometre scale) polymer fibers oriented in the fiber length direction. Nanofibers are characterized by high porosity and high surface-volume-ratio and physicochemical properties change is expected to affect the actuation driving process. As claimed in [2] clever usage of materials with reconfigurable, adaptive, and/or tunable physicochemical properties will be a key enabler in the field of soft robotics. Moreover, electrospinning allows producing a soft, biocompatible and lightweight material.

Contribution

This thesis proposes an electromechanical characterization set-up for the evaluation of force and displacement of a nanofibrous polyurethane-based soft actuator and to realize a model with the experimental data through the nonlinear system identification theory using an MLP neural network to identify the link between the electrical input voltage and mechanical output of the actuator. The obtained model has been used to perform a control system for the soft actuator, and a robotic arm application is proposed. Moreover the performance of the bundle, in term of comparison between electrical power dissipated and mechanical power produced, has been analyzed and compared to the performance of a DC linear motor. From the comparison, is clear the better performance of the bundle in terms of weight and power consumption.

The work is organized as follows: first section *Application* aims to identify the nonlinear model of the polyurethane-based soft actuator. The second part, *Application* makes uses of the nonlinear model identified to build a position control law. The second part ends with a possible future application of the soft actuator and energy analysis is presented.

Part I

ACTUATOR

Polyurethane as actuator

This section focuses on the background used for the electromechanical tests and on nonlinear system identification. It is shown how a polyurethane-based soft actuator is produced. Then a model identification for the nonlinear system is explained passing through optimization theory for the neural network application. This section ends with the application nonlinear system identification theory using neural networks, showing the results obtained in two study cases.

Chapter 1

Literature

1.1 Electrospinning

Electrospinning is a fiber spinning technique able to produce fibers of nanometric diameter starting from a polymeric solution. This process is possible thanks to high potential voltage that allow the fiber stretching. The general setup for the electrospinning includes a high voltage power supply, a spinneret, a grounded collected plate, and a syringe. The polymer solution is contained inside the syringe, pulled by electronic control. This movement pushes the solution thought the spinneret. Since the spinneret is connected to high potential voltage and the plates grounded, the solution starts to be stretched from the spinneret to the plate. This procedure allows the creation of nanofibers on the plate. Figure 1.1 shows how the electrospinning works. There are other types of setup configuration for other types of fiber production. The one used for the production of the bundle tested in this thesis is the one that uses instead of plates a rolling cylinder. As well as the plate, also the rolling cylinder is grounded. While in the case of the plates the fibers were deposited randomly, with the cylinder, rotating at high velocity, the fibers are aligned.

As said, the process of electrospinning is conducted under a high voltage. This high voltage produces a high electric field. The solution, pushed by the syringe through the pipe, it arrives at spinneret as a drop. When the magnitude of the electric field increase, the drop modifies its shape. Changing the shape, the droplet becomes a jet of solution. When this happens, on the spinneret, it creates a cone shape defined as Taylor cone. The jet created “flies” to the grounded cylinder: the solvents, added into the solution, evaporate when in contact with the air. This gives a pure polymeric filament. [10]

1.2 System Identification

This section provides some background on the theory of the system identification (SI) field. It describes how to identify a system focusing on the nonlinear system identification since the

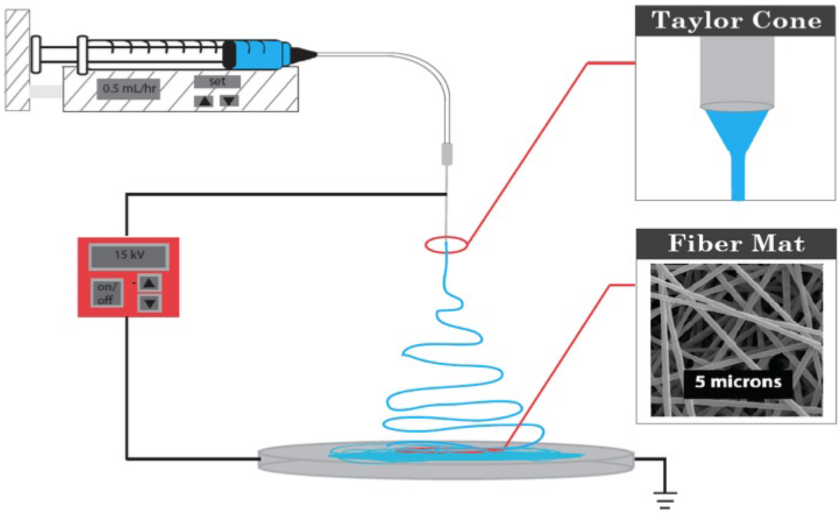

Figure 1.1: General setup for electrospinning process

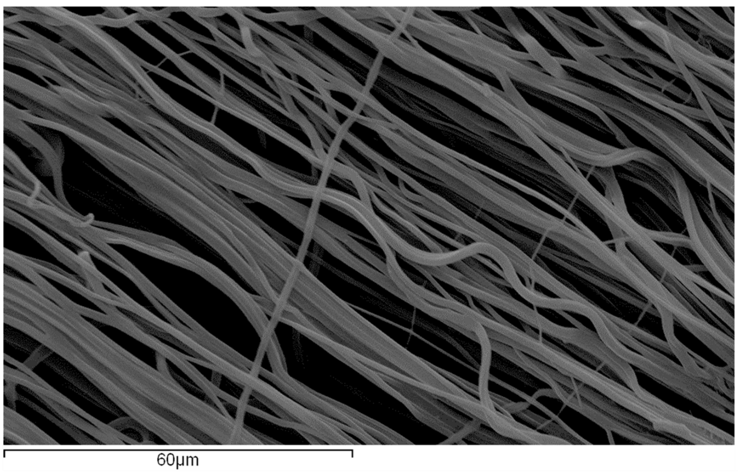

Figure 1.2: A SAM image of a polyurethane nanofiber

physical system studied presents some nonlinear behaviour. A way to identify nonlinear system can be the one using the theory of the *neural network*. Together with neural network theory, it is exposed also the optimization field with the focus on the gradient-based algorithm used for neural network training.

System identification field aims to understand and find a mathematical dynamical model for the physical system. A scheme of a general dynamic system is shown in figure 1.3 From

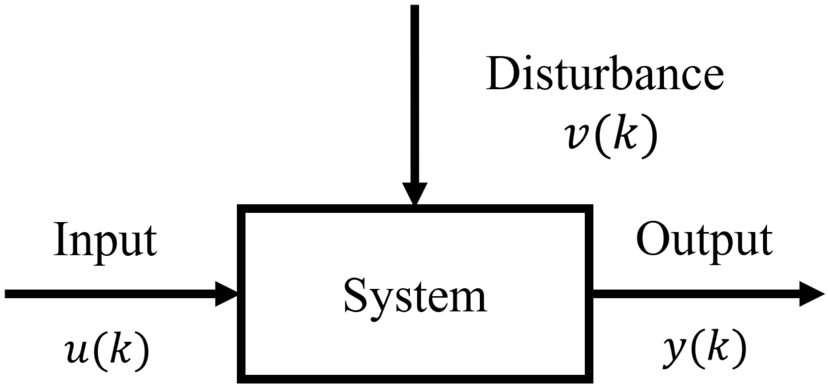

Figure 1.3: Dynamic System general representation

the figure is possible to notice that the system is driven by an input $u(k)$, and affected by a disturbance $v(k)$. The output is the system dynamic response to a certain input and a certain disturbance. In general for a dynamic system, the control action applied at time k affects the output at time $s > k$. A model of a physical system is useful on the engineering point of view: a model can be used to analyse the system, to obtain more information useful to predict or simulate the system behaviour. Furthermore, a model can be used to design a good control law. The way to a model of the physical phenomena can be of two types:

- *Mathematical modeling*. This approach is based on the idea to describe the dynamics of the system using the known laws from physics. This is an analytic approach.

- *System identification*. This method is based on the data. It starts injecting in the system some known input and sampling the output. This method aims to find the right value of the system parameters such that the data are consistent.

The system identification method is preferred when the physics of the system is too complex to be described just by physical insight. Respect to the mathematical modelling, the SI presents a limited validity. It can be applied only in certain working points and under certain assumptions.

Figure 1.4 shows a system identification procedure. It starts with the definition of the problem to be identified. Then the input used to excite the system is sampled together with the response of the system. Once the data has been collected, it is important to choose a suitable model structure. Then it follows the estimation of the unknown parameters of the model. To check if the estimated model is a good representation of the real one, a test is performed. The test is defined in the scheme in Figure 1.4 as a validation step, where if the found model doesn't

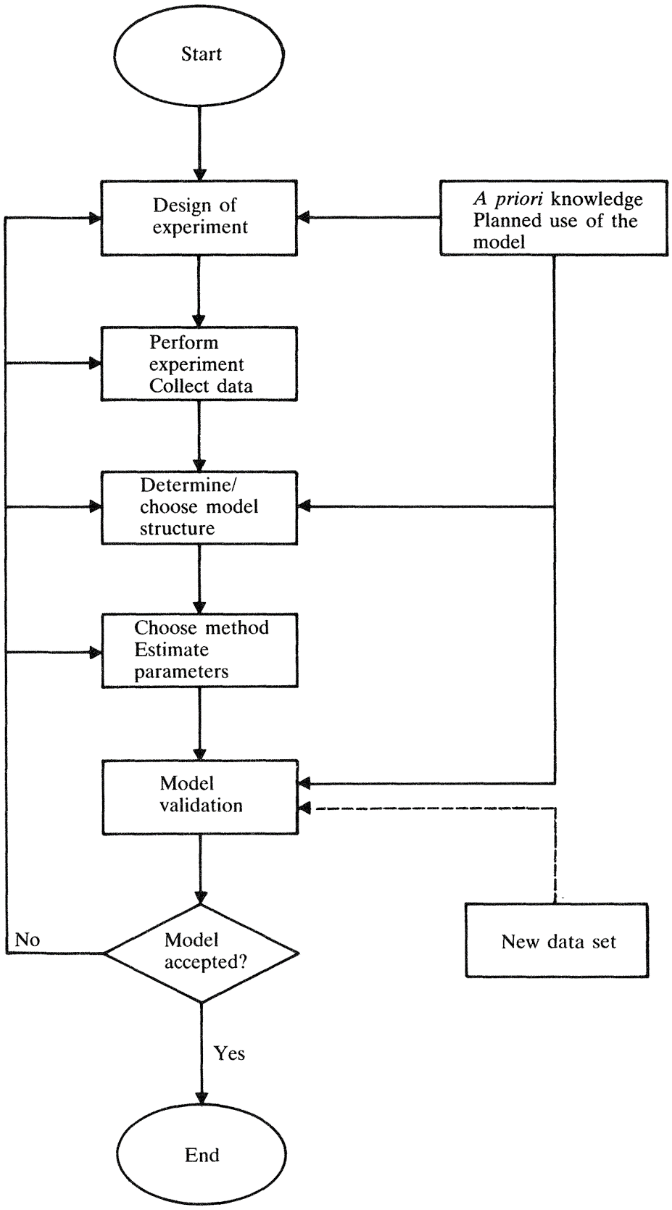

Figure 1.4: System identification flowchart

respect the constraints defined, a new identification model has to be used, and the flowchart starts again.

When the model of the system has to be chosen, it is a good practice to stat with the identification through a *linear* model. Then if this one doesn't satisfy the constraint and the behaviour expected, it means that inside that physical system are some nonlinear dynamics. Switching to the nonlinear model, sometimes doesn't mean better performance: if the system is not chosen enough flexible, it could be even worst then the linear one.

Based on the prior knowledge and the physic insight one can distinguish between three different types of model approach [13]:

- *White-box models*.This case occurs when all the dynamics of the process are well known, and it is possible to describe the dynamics with a mathematical model.
- *Grey-box models*. This case occurs when some physical insight is known but some parameters have to be estimated from experimental data.
- *Black-box models*. This case occurs when there is not physical insight, so both the model and the parameters are determinate on experimental data.

The *grey-box model* advantages and drawbacks are in between the white and black box, giving a good compromise between the two parts.

1.2.1 Nonlinear black-box identification

Let the general discrete-time input/output model, defined as *autoregressive exogenous input* (ARX) model be:

$$\hat{y}(k) = b_1 u(k-1) + \ldots + b_m u(k-m) - a_1 y(k-1) - \ldots - a_m y(k-m) \tag{1.1}$$

where b_i and a_i are scalar parameters, with $i = 1 \cdots m$, $\hat{y}(k)$ is the estimated output and $u(k-m)$ and $y(k-m)$ are the delayed input and output. It is possible to extend the same approach to the nonlinear case, obtaining the NARX (nonlinear ARX) where instead of the linear relation (1.1) , input and output delays are connected by a unknown nonlinear function $f(\cdot)$:

$$\hat{y}(k) = f(u(k-1), \ldots, u(k-m), y(k-1), \ldots, y(k-m)) \tag{1.2}$$

The concept of estimate the parameters a_i and b_i are extend to the accurate estimation of the function $f(\cdot)$. The family of model that describe the link of *input* and *output* is define *external dynamics*. There is also the so call *internal dynamics* approach that describes a system using the discrete state space equation approach. In this thesis the *external dynamics* approach has been used. As shown in Figure 1.5, the nonlinear model can be split into two parts: a nonlinear static approximation and an external dynamic filter, from here the name *external dynamics*. In

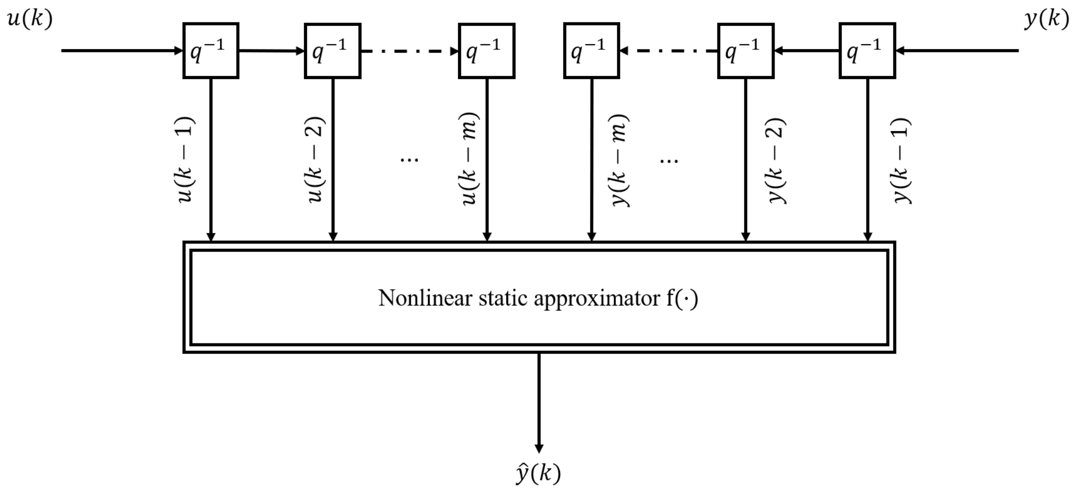

Figure 1.5: Nonlinear system discrete-time representation

general, the filter is chosen as simple delay q^{-1}. Moreover, the collection of more than one delay is defined as *tapped-delay lines*. The function $f(\cdot)$ can be chosen among different types, but in this work, the $f(\cdot)$ as been selected to be a neural network. A neural network is suitable for the purpose of this thesis since they can be used for the approximation of a nonlinear function [7]. As defined in the system identification section, a model prediction can be suitable for different purposes. In the case of the dynamic model, it can be used in two configurations, for prediction and simulation. The first one is suitable, as the name says for prediction, meaning that having the process input $u(k-i)$ and process output $y(k-i)$ the model provides the prediction of the output in several steps ahead. On the other hand, in the simulation approach the prediction is based only on the input $u(k-i)$ and the output predicted by the model. From [7], one can distinguish between serial-parallel referring to the one-step prediction configuration, and parallel mode for the simulation configuration. Figure 1.6 shows how the two configurations differ one to the others. The simulation configuration instead is suitable for scenarios where the output cannot be directly measured or also for fault detection. Other difference between the two approaches is the training mode. Both the models are trained by the minimization of a loss function dependent by the error $e(k)$. While in serial-parallel approach the error $e_{sp}(k)$is called equation error, in the parallel mode the error $e_p(k)$ is define as output error. Therefore, if a second-order model is considered, the predicted output for the one-step prediction model would be:

$$\hat{y}(k) = f(u(k-1), u(k-2), y(k-1), y(k-2)), \tag{1.3}$$

while the output simulated by the parallel model would be:

$$\hat{y}(k) = f(u(k-1), u(k-2), \hat{y}(k-1), \hat{y}(k-2)). \tag{1.4}$$

In this work, the focus is, as said at the beginning of this section, on the *external dynamics*, one-step prediction, meanly selecting as nonlinear static approximation function $f(\cdot)$ a particular

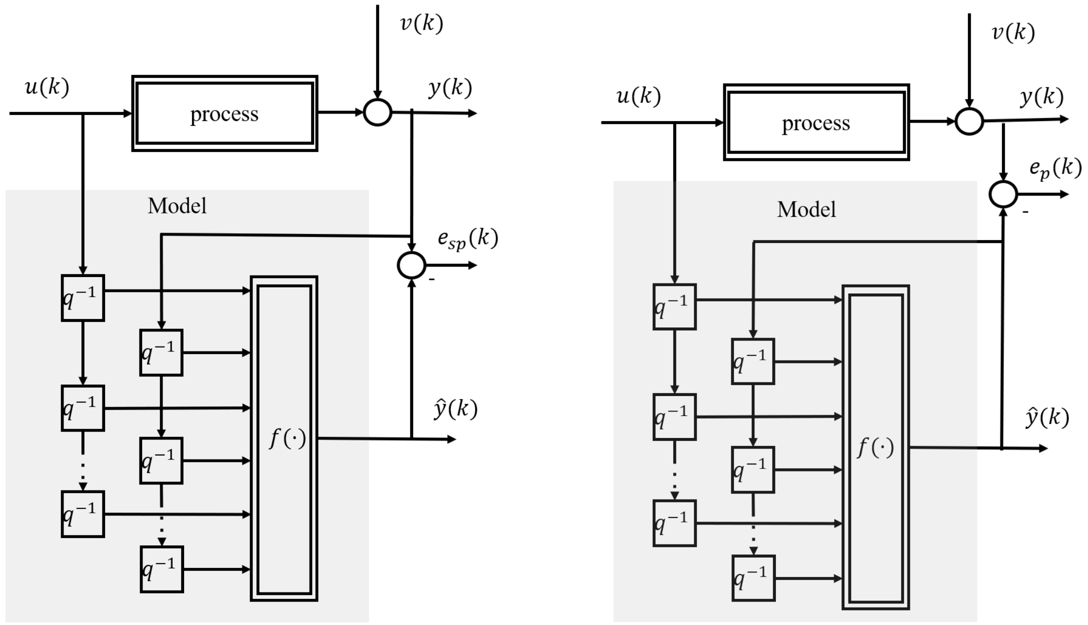

Figure 1.6: On the left the serial-parallel model for prediction. On the right side the parallel mode for simulation

structure of a neural network: *Multilayer Perceptron (MLP) network.*

1.3 Optimization

The concept of optimization yield to the idea of minimize (or maximize) some function. A general optimization problem is defined as [4]:

$$\begin{aligned} &minimize\ f_0(x) \\ &subject\ to\ f_i(x) \leq b_i,\ \ i = 1, ..., m. \end{aligned} \tag{1.5}$$

where the x is a vector with $x \in \mathbf{R}^n$ defined as the problem variable. The f_0 is defined as the *objective cost* function to be minimized, with the domain $f_0 : \mathbf{R}^n \to \mathbf{R}$. Then the $f_i : \mathbf{R}^n \to \mathbf{R}\ \ i = 1, ..., m$ are the *constraint functions* and the vector b collecting all the $b_i,\ i = 1, ..., m$ are the bound of the constraints. The aim of this optimization problem is to find a vector x^* that is the minimum under f_i constraints respect to the *cost* function.There exist four cases of optimal solution:

- x^* is a *global minimum* of f_0 if $f(x^*) \leq f(x)\ \ \forall x \in \mathbf{R}^n$
- x^* is a *strict global minimum* of f_0 if $f(x^*) < f(x)\ \ \forall x \neq x^*$
- x^* is a *local minimum* of f_0 if $B_\varepsilon(x^*) = \{x \in \mathbf{R}^n \mid \|x - x^*\| < \varepsilon\}$
- x^* is a *strict local minimum* of f_0 if $f(x^*) < f(x)\ \ \forall x \neq x^*\ and\ x \in B_\varepsilon(x^*)$.

It is possible to distinguish between two optimization problem based on the type of function to be optimized. When the cost to be optimized and the constraints are a linear functions, then the problem is called *linear program*. To be a linear program this condition must hold:

$$\begin{aligned} & f_i(\alpha x + \beta y) = \alpha f_i(x) + \beta f_i(y) \\ & \forall\, x, y \in \mathbf{R}^n \; and \, \forall\, \alpha, \beta \in \mathbf{R} \end{aligned} \tag{1.6}$$

When the cost function is nonlinear then the problem became a *nonlinear program*. In this thesis, *data fitting* is used. Indeed the aim of *data fitting* is to find the best model, among the available ones. In this case, the cost function can be assumed as the mismatch error between the observed data and the values predicted by the model. The constraint can be represented by the priory knowledge about the parameters system.

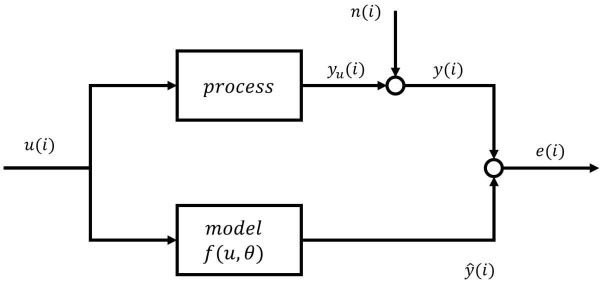

Figure 1.7: Error function for model estimation

Figure 1.7 represents how a cost function can be used: a model $f(\cdot)$ links the input vector to the output. The model is parameterized respect the vector θ such that $y = f(u, \theta)$. The aim of the optimization is to find the best approximation of $\widehat{y}$ respect the real one y. The only way to have a better approximation is to tune the parameter θ such the error $e(i)$ is the minimum possible.

The work to reduce the errors and, therefore, to tune the parameter vector θ is associated with the algorithm chosen. Considering the problem (1.6), the optimal solution will be found applying the general algorithm :

$$\begin{aligned} & x^{t+1} = x^t + \alpha^t d^{\,t} \\ & t = 0, 1, \ldots \\ & where\; \alpha^t > 0\;,\; (\alpha^t \;\in\; \mathbf{R}) \\ & and\;\; d^{\,t}\; such\, that\, if\; \nabla f(x^t) \neq, \nabla f(x^t) d^{\,t} \;<\; 0 \end{aligned} \tag{1.7}$$

The two variables α^t and $d^{\,t}$ are respectively the *step size* and the *direction* of the algorithm. Based on the choice of these parameters it is possible to get different converging algorithm. A general procedure to start an algorithm is:

1 select the direction $d^{\,t}$;

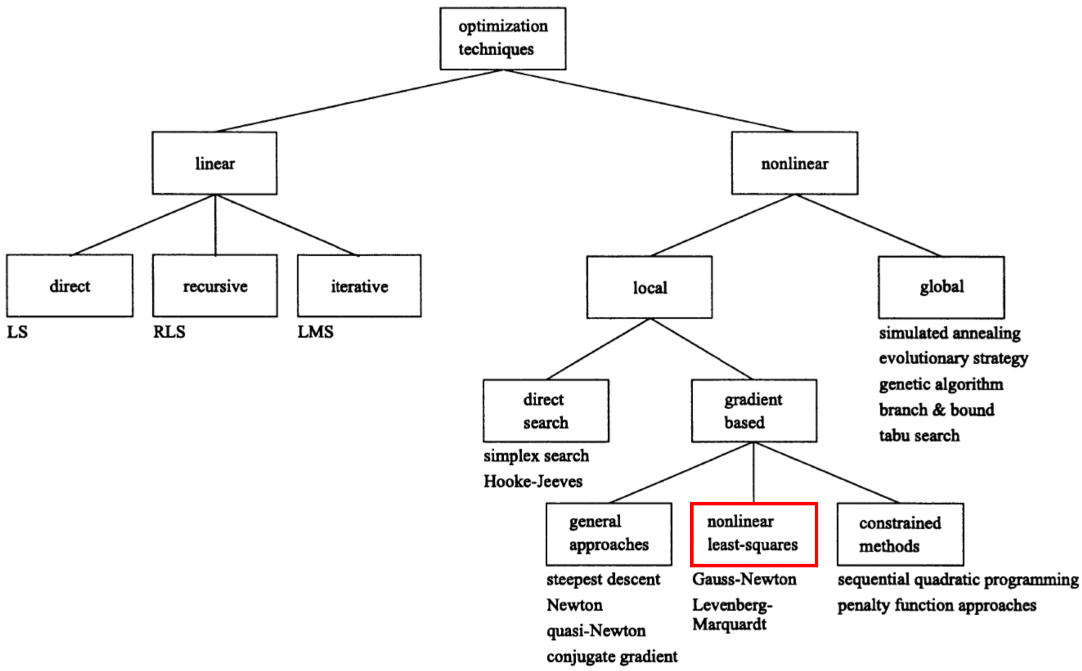

Figure 1.8: Optimization techniques classification

2 select the step size α^t.

Figure 1.8 well describes the different level of the converging algorithm: the first layer is composed of different types of cost function. It follows, in the branch of the nonlinear block, the classification based on the type of minimum. Next, considering the gradient base block, it presents three different choices. As highlighted from the figure, in this thesis has been used the *nonlinear least-squares* **Levenberg-Marquardt** optimization technique for neural network training. Before to describe the *Levenberg-Marquardt*, it is necessary to define the meaning of the nonlinear least square. As the name said, this methods is an extension of the classic least square (LS). The nonlinear LS has the advantage to be used with much larger and more general class of functions. The estimation of the parameters is conceptually the same as is in the linear LS. Equation (1.8) defines a general *nonlinear LS* problem with nonlinear parameters.

$$f(x) = \sum_{i=1}^{m} f_i(x)^2 \tag{1.8}$$

with f_i are a twice differentiable function. Next, the *gradient* and the *Hessian* of f at x can be computed:

$$\nabla f(x) = \sum_{i=1}^{m} f_i(x)\nabla f_i(x), \quad \nabla^2 f(x) = \sum_{i=1}^{m} \Big(f_i(x)\nabla f_i(x)^T + f_i(x)\nabla^2 f_i(x) \Big) \tag{1.9}$$

The nonlinear LS algorithm can be divided into two categories: small residual algorithm and large residual algorithm. The distinction is based on the approximation of the Hessian. In the first case it is considered just Hessian matrix $\nabla^2 f(x) \approx \sum_{i=1}^{m} f_i(x)\nabla f_i(x)^T$. This condition hold only if $f_i(\cdot)$ is small, which is the case of choice done in this thesis. Usually, the function consider is represented by the radius error so the previous condition holds. Before to proceed let's define Jacobian and Hessian under vector notation:

$$J = \nabla f(x), \quad H = \nabla^2 f(x) \approx J^T J \tag{1.10}$$

Coming back to the *descent algorithm* $\big(1.7\big)$, as said, it needs the selection of the direction $d^{\,t}$. Selecting an direction of this type :

$$d = \left(JJ^T + \beta I\right)^{-1} J^T f \tag{1.11}$$

a **Levenberg-Marquardt** is obtained. The iterative algorithm became:

$$x^{t+1} = x^t + \alpha^t \Big(J^t (J^t)^T + \beta^t I^t\Big)^{-1} (J^t)^T f^t \tag{1.12}$$

The Levenberg-Marquardt is basically an extension of Gauss-Newton algorithm. Starting from Levenberg-Marquardt is possible to approximate the Gauss-Newton algorithm using small value of β^t. Setting large value of β^t the algorithm behaves like steepest descent.

This algorithm has been used to train the neural network in the experimental chapter.

1.4 Neural Networks

An artificial neural network, in general, is composed of a basic unit defined as *neuron*. The name *neural* comes from the inspiration to the human and animal brain [7]. Based on this idea it has been translated and build something similar in mathematical terms. Even if the difference between the real neuron and the artificial one is slightly different, the general idea is similar. Indeed the two neurons had in common some characteristics: a large number of simple units, highly parallel units, strongly connected units, fault-tolerant concerning the failure of a single unit, learning from data. A neural network can have a ridge construction, radial construction or tensor product construction. In this work, it has been considered the *rigid construction*. Among these categories, the widely known one is the *multilayer perceptron network* . The basic unit of an MLP is the *perceptron*. It is composed, as shown in Figure 1.9, by two-part. The first part is composed of the union of the weighted input vector elements. The second part takes the result of the first part, and it projects them though a nonlinear function $g(x)$ obtaining the perceptron output. There are different classes of nonlinear functions, all are saturation function. The function can be *sigmoid, logistic,* and *hyperbolic tangent*. To obtain one hidden layer network it is needed the same input on M parallel perceptrons (figure 1.10). The output is the combination of the perceptron outputs and can be computed considering:

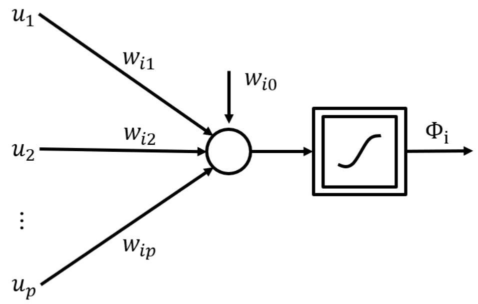

Figure 1.9: Schematic representation of a perceptron

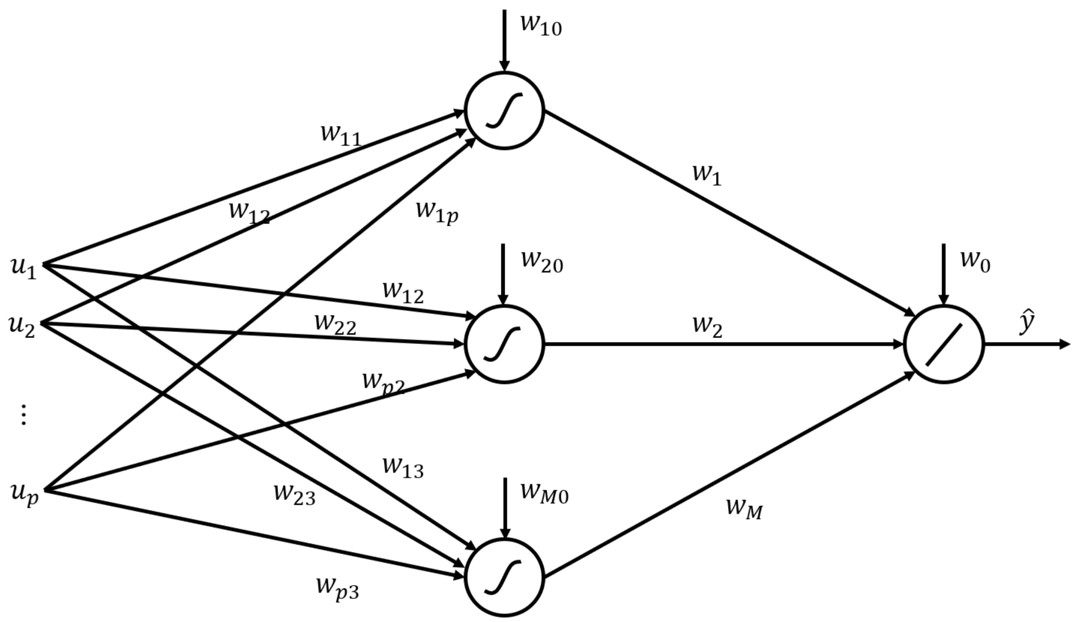

Figure 1.10: A general one hidden layer network

$$\hat{y} = \sum_{i=0}^{M} w_i \Phi_i \left(\sum_{j=0}^{p} w_{ij} u_j \right) \text{ with } \Phi_0(\cdot) = 1 \text{ and } u_0 = 1 \tag{1.13}$$

where w_i are the output layer weights and w_{ij} are the hidden layer weights.

An MLP network can approximate any smooth function. More perceptrons are added more the accuracy increases. In general, an MLP network is characterized by two types of parameters: output layer weight and the hidden layer weight. The first parameters are linear and they establish the amplitudes and the basis function at the operating point. The second, instead, are nonlinear parameters and they define the direction, the slop and the positions of the basis functions. To approximate any smooth function, these parameters have to be tuned. A way to tune them is optimality. The backpropagation is the optimization algorithm used to tune those parameters. Backpropagation is a method for gradients computation on an MPL network. Considering an MLP network with M hidden layer weight, then the derivatives of the MLP output with respect to the output layer weight are:

$$\frac{\partial \hat{y}}{\partial w_i} = \Phi_i \quad \text{with } \Phi_0 = 1 \text{ and } i = 1, \ldots, M \tag{1.14}$$

Next the derivative of MLP output with respect to the hidden layer weights are:

$$\frac{\partial \hat{y}}{\partial w_{ij}} = w_i \frac{dg(x)}{dx} u_j \quad \text{with } u_0 = 1 \text{ , } i = 1, \ldots, M \text{ and } j = 1, \ldots, p \tag{1.15}$$

for every weight from the jth input and the ith hidden neuron. The name backpropagation come because the gradient expression is constructed by propagating the model error back through the network. The main algorithms to apply the backpropagation are:

- Regulated activation weight neural network (RAWN),
- Nonlinear optimization of the MLP,
- Staggered training of the MLP.

In this work it has been used the second one.

Chapter 2

Setup and methods

2.1 Setup

The electromechanical characterization has been performed with the test instrument Instron™ ElectroPuls E1000 (`www.instron.us`), equipped with the Instron™ static load cell 2530-5N, which has a capacity of ± 5 N and a sensitivity of 1.6 mV/V to 2.4 mV/V at static rating. The measurement set-up is depicted in Figure 2.1.

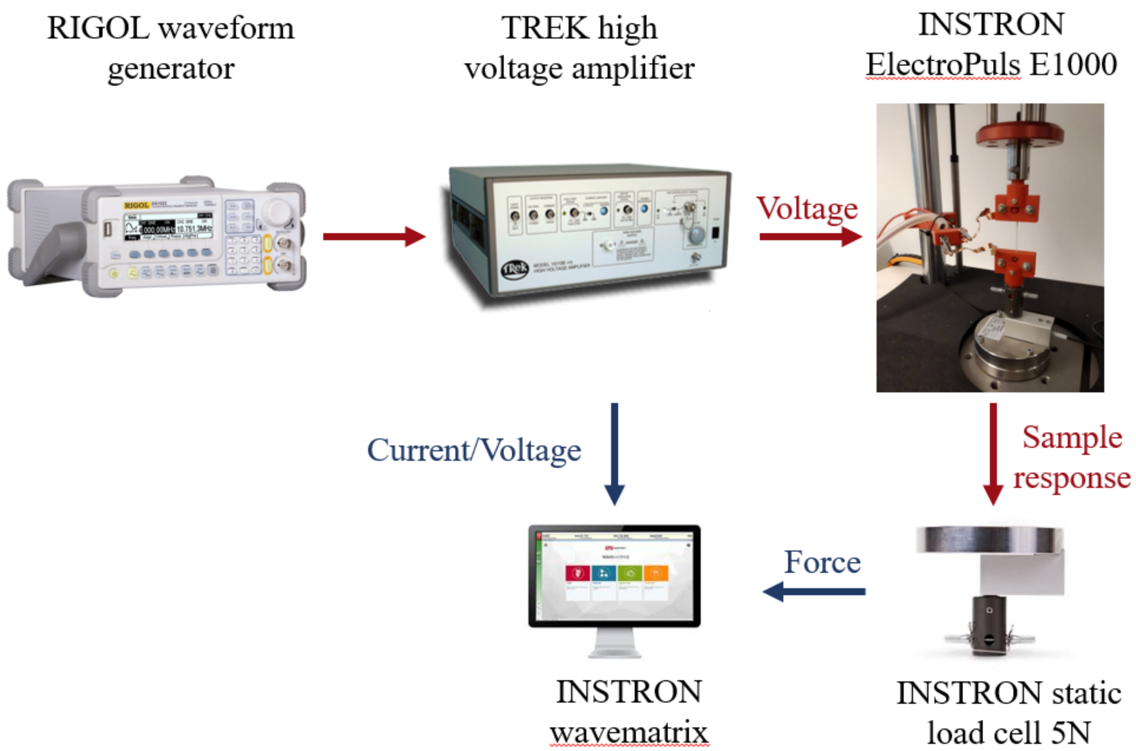

Figure 2.1: Measurement set-up for the electromechanical characterization of the soft actuator: the Instron™ ElectroPuls E1000 receives voltages as inputs and registers the response of the specimen (either a force or a displacement). The Instron™ wavematrix software collects the generated data.

The specimen is placed inside the Instron testing instrument and clamped with two grips, which have been 3D-printed in ABS material. The surfaces of the grips are covered with copper tape and connected to a TREK 10/10B-HS high-voltage amplifier (`www.trekinc.com`) through crocodile plugs, in order to apply a voltage to the specimen. The high-voltage generator is controlled by a RIGOL DG1022 input waveform generator (`www.rigolna.com`).

The test instrument Instron™ ElectroPuls E1000 is either controlled to maintain a fixed displacement (the extremities of the bundles are kept at a constant distance) to measure the axial contraction force, or to maintain a fixed force to measure the axial displacement. The data are collected at $1\ [KHz]$, by using two strain channels connected to the Instron™ ElectroPuls E1000, and analyzed in a desktop PC through the Instron™ Wavematrix Software. The two strain channels are used to record the displacement or the force, the voltage, and the current that flows through the specimen when the voltage is applied.

2.2 Bundle setting up

The beginning of each experiment, either the displacement of the force test, starts with the selection of the bundle to be tested. In this work, it has been selected the polyurethane nanofiber mixed with TABF [1] salt in a concentration of 10%. The PU its self is a non-conductive material. When the solution is prepared for the electrospinning, together with the PU is added salt in a concentration of 10%. The nanofiber created is still not entirely conductive, due to the only 10% of conductive material. To overcome this problem the nanofiber is soaked in a solvent: the polycarbonate (PC). The soaked mixed nanofiber obtained is a conductive bundle.

The procedure before to start each test is shown in Figure 2.2. The procedure is divided into different steps. The bundle arrives in a ring shape, Figure 2.2 step (a). Next, a piece of this ring is taken. It has been cut a slice of length $40\ [mm]$ step (b). Then is weighted and the section is measured, resumed in the table 2.1. Once all the dimension of the bundle is measured, the soaking procedure is performed Figure 2.2 step (c).

It has been fixed time of soaking of $30\ [s]$. This is the time needed for the PC to reach all the nanofibers into the bundle. Immediately after the soaking step, the bundle is dried in a filter paper (step (d)). This step is fundamental otherwise the salt swells out the nanofibers.

Step (e), in Figure 2.2 defines the last procedure before the beginning of the test: the bundle is fixed in both the sides by two conductive clamps. The clamps, internally covered of copper

[1] tetrabutylammonium

LENGTH	$40\ mm$
SECTION	$0.6\ mm$
WEIGHT	$0.007\ g$

Table 2.1: Dimension bundle

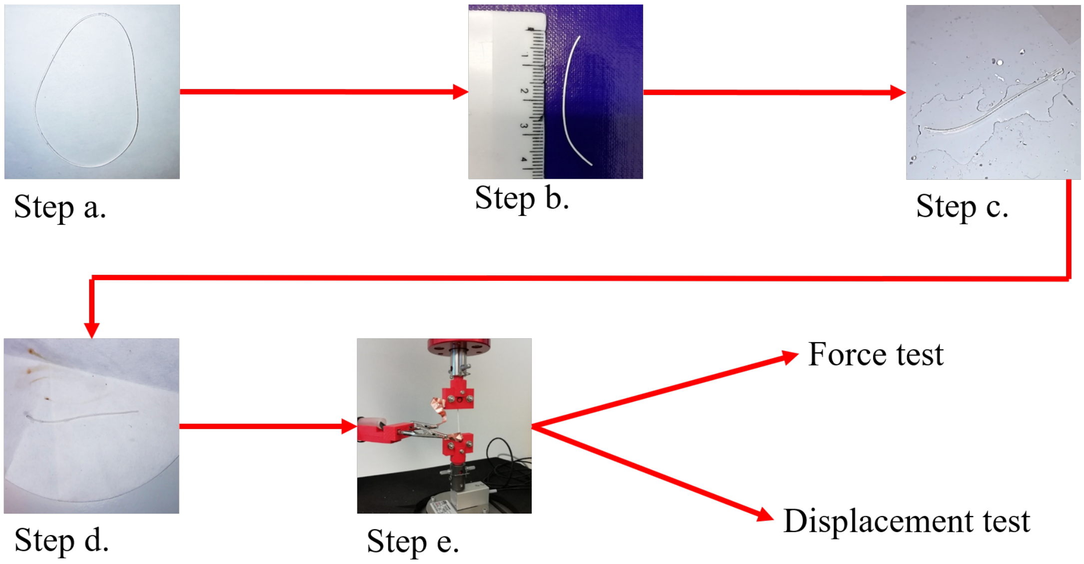

Figure 2.2: Bundle preparation for displacement and force test

tape, to apply a voltage at extremities of the bundle.

The clamps together with the bundle are then mounted to the Instron machine: one clamp is attached to the fixed part of the Instron machine (upper part), while the other one is linked to the load cell (down part). At this point using the manual control of the Instron machine, the bundle has been set under a preload of $0.2\ [N]$. Due to the pretension, the bundle was straight in the vertical direction. Before the beginning of the test, it has been noticed a negative drift in the preload measured by the load cell. This was due to the internal relaxation of the nanofibers. To have a stable measurement of the force by the load cell, it has been decided to wait for 10 minutes before the beginning of each test. After the last step, one of the two tests has been performed.

2.3 Matlab Neural Network toolbox

Matlab [8] illustrates a workflow for neural network design. First of all, collect the data of the system to analyze. In general, this procedure occurs outside of the NN toolbox software. Next, it must be created the network, under certain choices that will discuss later. After the creation, the network is configured with the proper parameters: numbers of input delays, numbers of hidden layers and numbers of neurons are selected according to the experiment. It follows the initial training of the network. At the end of the procedure is performed a validation using part of the data collected as a tester. There are four types of access to the NN toolbox. Among those, in this thesis it has been used the “command-line” approach, using a Matlab script.

As defined in the section of the neural network, the base component is the neuron. In the

Matlab environment, a basic neuron is described by the function

$$a = f(wp + b) \tag{2.1}$$

where p is the input (scalar in this example), w is the weight and b is the bias. Figure 2.3 shows Matlab neuron representation. Important is the function $f(\cdot)$ defined as transfer function. It

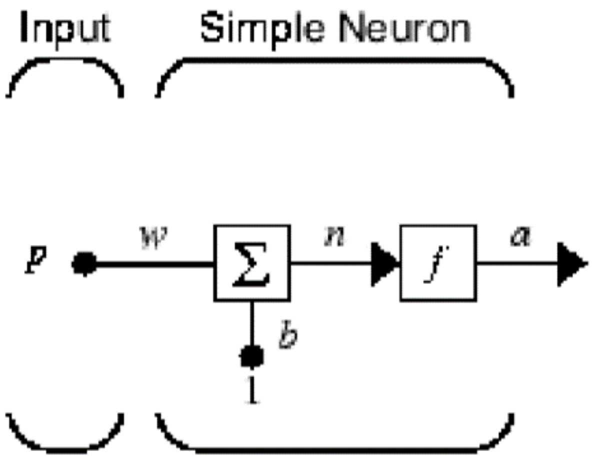

Figure 2.3: Matlab neuron representation

can assume different type of function. Moreover the function $f(\cdot)$ produces the (scalar in this case) output a. An important property of the neurons is that can either w and b can be adjustable such that a particular behaviour is obtained by the entire neural network. The idea of the scalar neuron can be extended the usage of vector input (*dimension* Rx1). The formula 2.2 define the case of the vector as input.

$$a = f(\mathbf{Wp} + b) \tag{2.2}$$

This time, respect to the scalar case, the weight is not anymore scalar but is a matrix. Indeed the vector **p** is then post-multiply by the **W**. As in the scalar case, also in this case a bias b (scalar) is added. If more then one neurons are taken such that each neuron has the same input vector then a *One layer of Neurons* is obtained. The lantern is composed of the same vector of input but, differently from one single neuron, the output and the bias are vectors. Adding more then *One layer of Neurons* in cascade, meaning that the output vector of one layer is the input of the next one, gives the composition of *Multilayers of Neurons*. Each layer is characterized by its weight matrix and bias vector. The NN toolbox gives the possibility to choose the structure of the network, in particular, one can choose between two types of input vectors: *concurrently* and *sequentially*. The first is the simplest case of network: it presents no delay in the input and no feedback. Moreover, the order of the elements of the input vector doesn't matter. The dynamic case, instead, contains delay and the input vector is a sequence with a certain time order. The NN toolbox allows selecting between two modalities of training: incremental and bash. In the first case, the gradient and the weight computed are updated after each input is applied to the network.

In the bash mode, all the input are applied to the network before the weights are updated.

2.4 Matlab System Identification Toolbox

Among Matlab toolboxes, it has been used in this thesis also the system Identification toolbox. From [14], System Identification Toolbox provides MATLAB functions, Simulink blocks, and an app for constructing mathematical models of dynamic systems from measured input-output. It is possible to identify the system dynamics of a complex system using only the data sampled. The input-output data can be either time-domain or frequency-domain to identify continuous-time or discrete-time transfer function, process model and state-space model. Figure 2.4 shows the user interface of the toolbox. On the left side, there is the location for the input-output

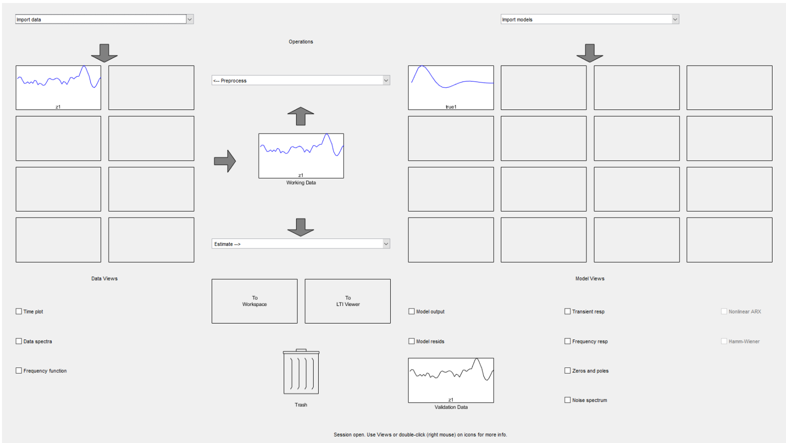

Figure 2.4: Matlab system identification toolbox interface

data upload. Once the data are uploaded, it is possible to perform some pre-processing step i.e. *Remove mean*, *Remove trends*, *Resample* , and *Filter*. There are different type of identification: from the linear one through transfer function, passing from the nonlinear with the NARX model. Depending on the type of system identification, there are some parameters to be chosen. In the case of *transfer function* the parameters to be selected are the numbers of *pole* and *zero*. Once all the settings are ready the estimation of the parameter is performed. The identified function appears in the windows on the right of the user interface (Figure 2.4). From this user interface is possible to compare the real output with the estimated transfer function output. When the model estimated satisfies the requirement of the user, it can be exported to the Matlab workspace

Chapter 3

Experiments

In the experiment chapter, it has been applied the theory of the nonlinear system identification using the neural networks. Specifically, it has been identified the model of the PU plus salt as an actuator. The test performed is divided into two parts: in the first part the bundle is clamped to the Instron machine and the data of voltage and force are sampled. The second part instead aims to control the force applied to the bundle and sample voltage and displacement.

3.1 Force sampling, displacement control

The force test aims to understand the PU plus salt behaviour under a certain applied voltage.

The experiment starts applying a preload to the bundle of $0.2\ [N]$. Then the idea was to perform a displacement control, such that the distance between the two clamps was constant in time. The Instron machine was in charge to hold the gauge distance. While this control was performed, the load cell was sampling the force provided by the bundle under a certain voltage.

It has been decided to perform three different signal input test:

- Two squares input of voltage of 100 and $200\ [V]$ figure 3.1a ;
- A trapezoidal shape with pick of $300\ [V]$ figure 3.1b;
- A sine wave of period $30\ [s]$ bias $125\ [V]$, amplitude $250\ [V]$ figure 3.1c.

The signals just mentioned were obtained through the wave generator RIGOL DG1022, in combination with the amplifier. Indeed, as defined by Figure 2.1 , the wave generator gave a signal in mV raised to V by the amplifier TREK MODEL 10/10B-HS.

After the windows of 10 minutes for cell load stabilization, the force measured has been reset to zero. Then the first test has been performed. The Instron machine allows sampling concurrently both the force on the load cell and the voltage applied to the bundle. The two signals have been sampled at the frequency of $1\ [kHz]$. Once the three tests have been performed, the Instron machine has been saved the sampled data in .CSV format. The data have been then processed and saved in an excel file. The latter file has been composed of two-column cells for

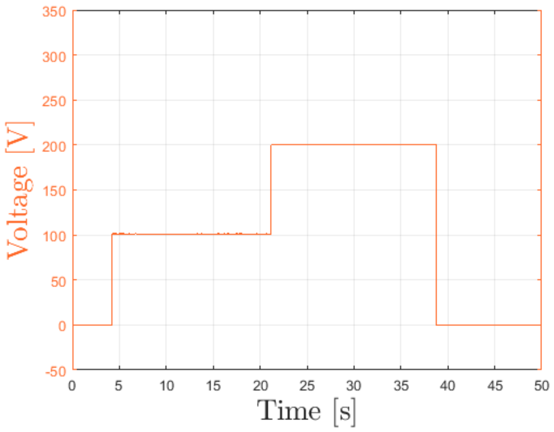

(a) Squares input

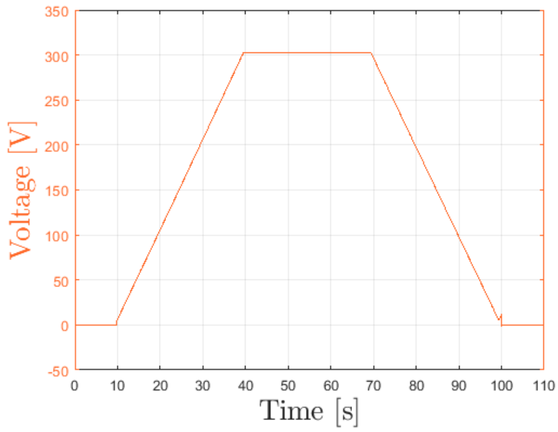

(b) Trapezoidal input

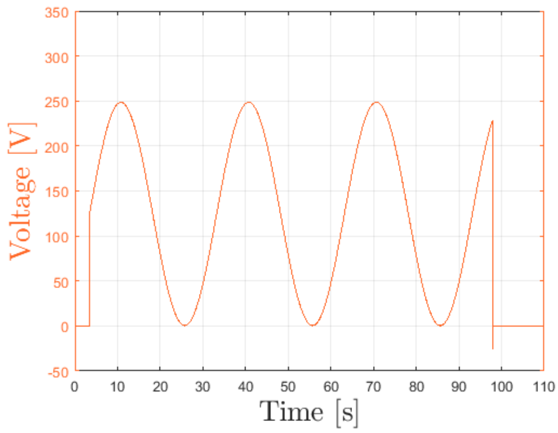

(c) Sine input

Figure 3.1: Different input Voltage signals.

each couple of input (Voltage) and output (Force). Figure 3.2 shows the force sampled by the Instron, in response respectively to squares (Figure 3.1a), trapezoidal (Figure 3.1b) and sine (Figure 3.1c) voltage stimuli. From Figure 3.2 is possible to notice how the bundle reacts (force measurement) to an input stimulus (voltage).

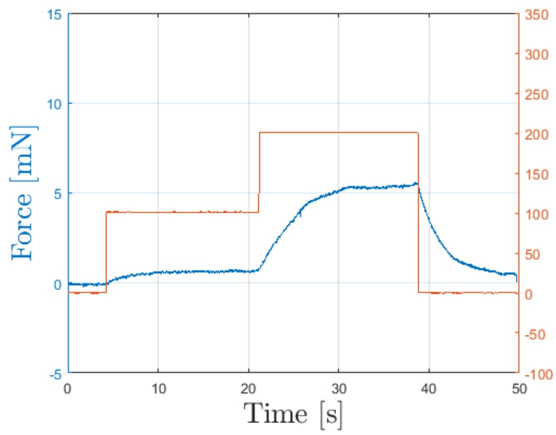

(a) Squares output

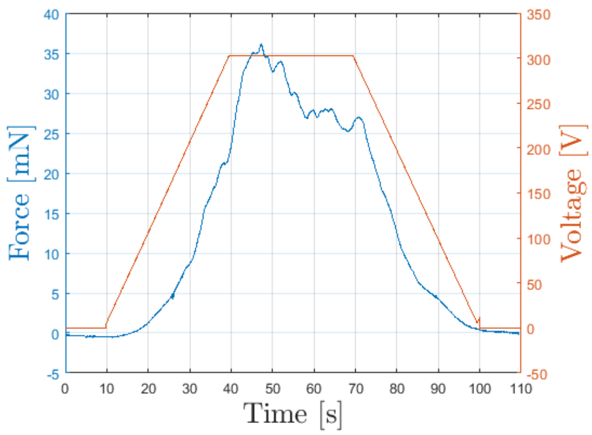

(b) Trapezoidal output

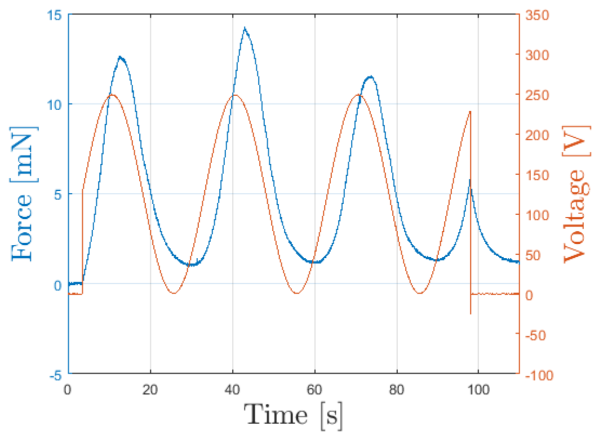

(c) Sine output

Figure 3.2: Input/output sampled data. Force test.

Having the sampled data the identification part has been executed. To perform a system identification, it has been created a Matlab code defined in the following:

- *MAIN.m* the script, the core of the code identification;
- *Import_data.m* responsible for the upload of the sampled data from the excel file to the Matlab work-space;
- *NN_narx_exe_V_F.m* with the aim to initialize and perform the neural network identification.

When the *MAIN.m* is launched, the sampled data of input-output of each of the three signals are upload in vectors using the script *Import_data.m*. In the same script has to be define the input

Type NN	NARX feedforward-closed loop
# HIDDEN LAYERS	1
# OUTPUT LAYERS	1
# INPUT DELAYS	6 for y ; 6 for u
# NEURONS HIDDEN	10
MINIMUM GRADIENT	$1e-11$
TRAINING METHOD	trainlm (Levenberg–Marquardt)
FUN. HIDDEN LAYER	sigmoid
FUN. OUTPUT LAYER	linear

Table 3.1: Setting for neural network

vectors for the training part and those for the validation part. Moreover, the number of *delay input* and *output*, and the number of neurons for the neural network have to be specified. The *NN_narx_exe_V_F.m* script is contained in the *MAIN.m* and aims to set up the neural network and start the training with the sampled data. Table 3.1 shows the main features of the NN adopted. The script starts with the creation of a feedforward "NARX" net with one hidden layer composed by 10 neurons. The function used by the neurons to link the combination of the inputs, with the output of the hidden layer is a **sigmoid** function. The output of the sigmoid is then combined in a linear function to get the neural network predicted output. The NN created is shown in figure 3.3a. In the script *NN_narx_exe_V_F.m* has to be defined the setting of the minimum gradient limit within which the training process stops. If the training procedure doesn't reach the minimum gradient within the number of "epochs" defined, the training procedure will stop. By default, the training method is assumed as *trainlm* (Levenberg–Marquardt). Once all the settings have been set, the training command has been performed. When the NN has to be trained, it needs both the input and the output of the sampled data, that in force test are voltage and force. This configuration is called open-loop or feedforward network (figure 3.3a). When, instead, the output (force) has to be predicted starting from a known input (Voltage), a closed-loop NN has to be used. Closed-loop NN means an open-loop NN where the output predicted is used as feedback input. Figure 3.3b well illustrates a closed-loop NN. With the creation of the closed-loop NN, the script file *NN_narx_exe_V_F.m* finishes its job. Then is the *MAIN.m* that provides the command to extract a Simulink block from the closed-loop NN.

The usage of nonlinear system identification in these experiments comes from the behaviour of the bundle. It has been decided to perform also a linear identification of the model. The linear model was discharged because the nonlinear identification with the neural network just fit better the real data. To demonstrate what just claimed, a linear system identification has been performed using the Matlab toolbox System Identification. As defined in the method chapter, the toolbox presents the interface to, first upload the data, and then to use different modalities to identify the system. To be consistent, the same input data of the nonlinear identification has been used (Figure 3.2). It has been performed the linear identification through the transfer function

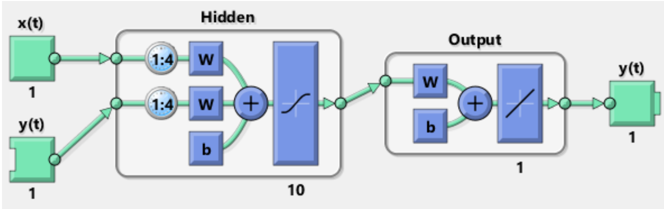

(a) Forward neural network

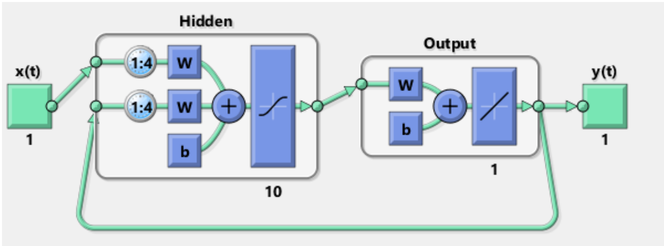

(b) Closed loop neural network

Figure 3.3: Matlab neural network representation.

parameters estimation. The best combination of number of *pole* and *zero* has been a transfer function with 7 poles and 5 zeros.

The transfer function has been:

$$T(s) =$$

$$\frac{-1.497^{-09}s^5 - 4.515^{-12}s^4 + 9.188^{-14}s^3 + 9.97^{-16}s^2 - 8.963^{-20}s + 7.637^{-23}}{s^7 + 1.56^{-2}s^6 + 3.25^{-4}s^5 + 4.19^{-06}s^4 + 1.556^{-08}s^3 + 1.349^{-11}s^2 + 1.509^{-15}s + 1.271^{-18}} \tag{3.1}$$

3.2 Displacement sampling, force control

The experiment for the displacement test aims to understand how the PU plus salt behaves under certain voltage signal. This time is examined the displacement of the bundle applying on the two sides of the bundle a constant preload of 0.2 $[N]$. Doing this test it has been defined the relation between the input *voltage* $[V]$ and the output in *displacement* $[\mu m]$. Different from the force test, in this test the Instron machine has performed a control on the force applied to the bundle. While the previews test was just asked to hold constant in time the gauge distance, in this test the Instron machine was performing a PID control of the force, holding it constant to 0.2 $[N]$. As well as the previous test, also in the displacement test have been used three inputs though the wave generator:

- two squares shapes of 100 and 200 $[V]$;
- a trapezoidal shape of peck of 200 $[V]$;
- a sine wave of period 30 $[s]$ and amplitude of 200 $[V]$.

Figure 3.4 shows the input and the output sampled in the displacement test.

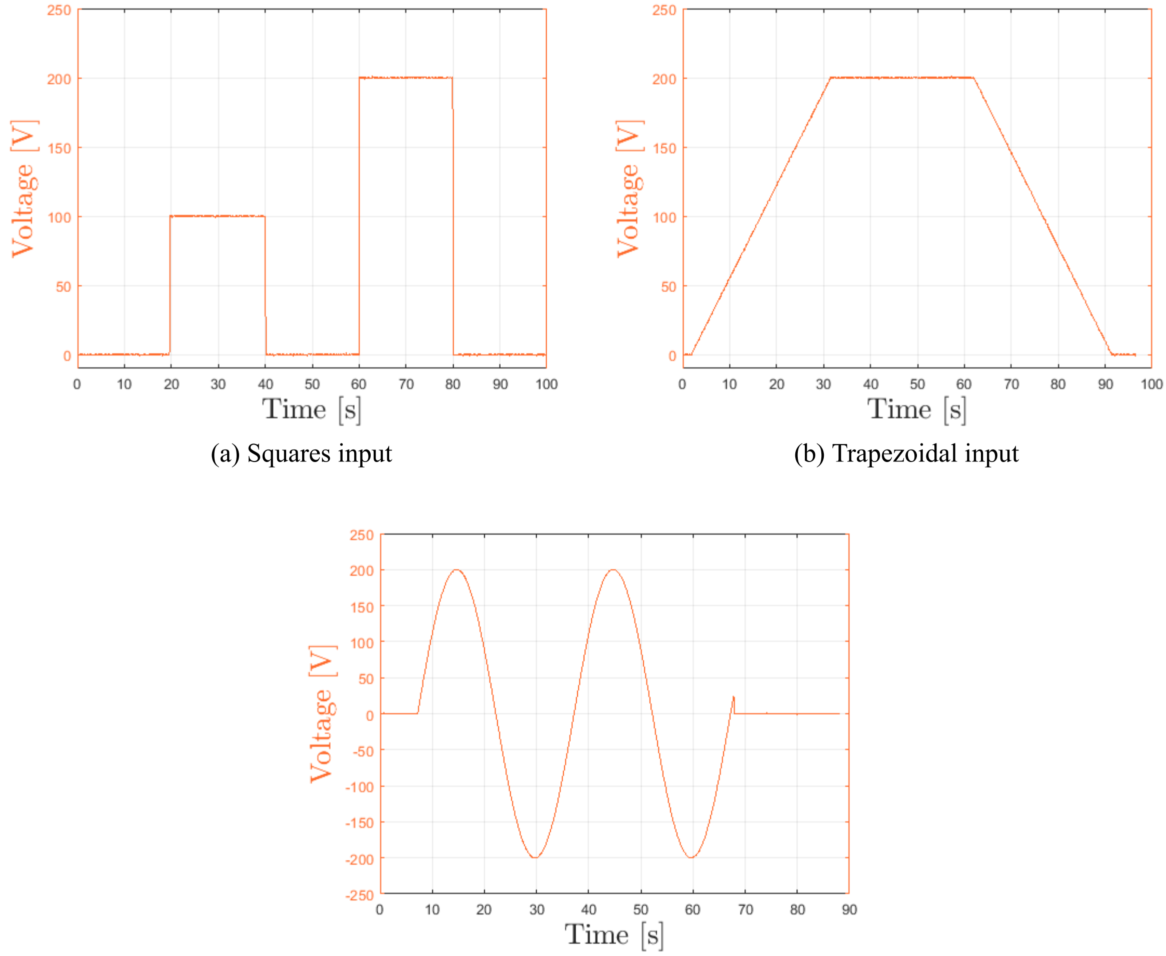

(a) Squares input

(b) Trapezoidal input

(c) Sine input

Figure 3.4: Input voltage signals

As defined in the *Bundle set up*, it has waited for 10 minutes for the cell stabilization. The preload of 0.2 $[N]$, it has been applied with a ramp of 10 seconds and then the experiment has been started. With a sampling frequency of 1 $[kHz]$ both the input (voltage) and output (displacement) have been sampled. In Figure 3.5 are shown the output displacement responses of respectively squares, trapezoidal and sine shape.

Once the sampling test has been finished, the identification part started. The idea of the identification is basically the same of the *force test*, but with some changes in the NN setting. As the input of the NN has been used the collection of the inputs and outputs sampled.

The table 3.2 resume the setting used in the nonlinear identification.

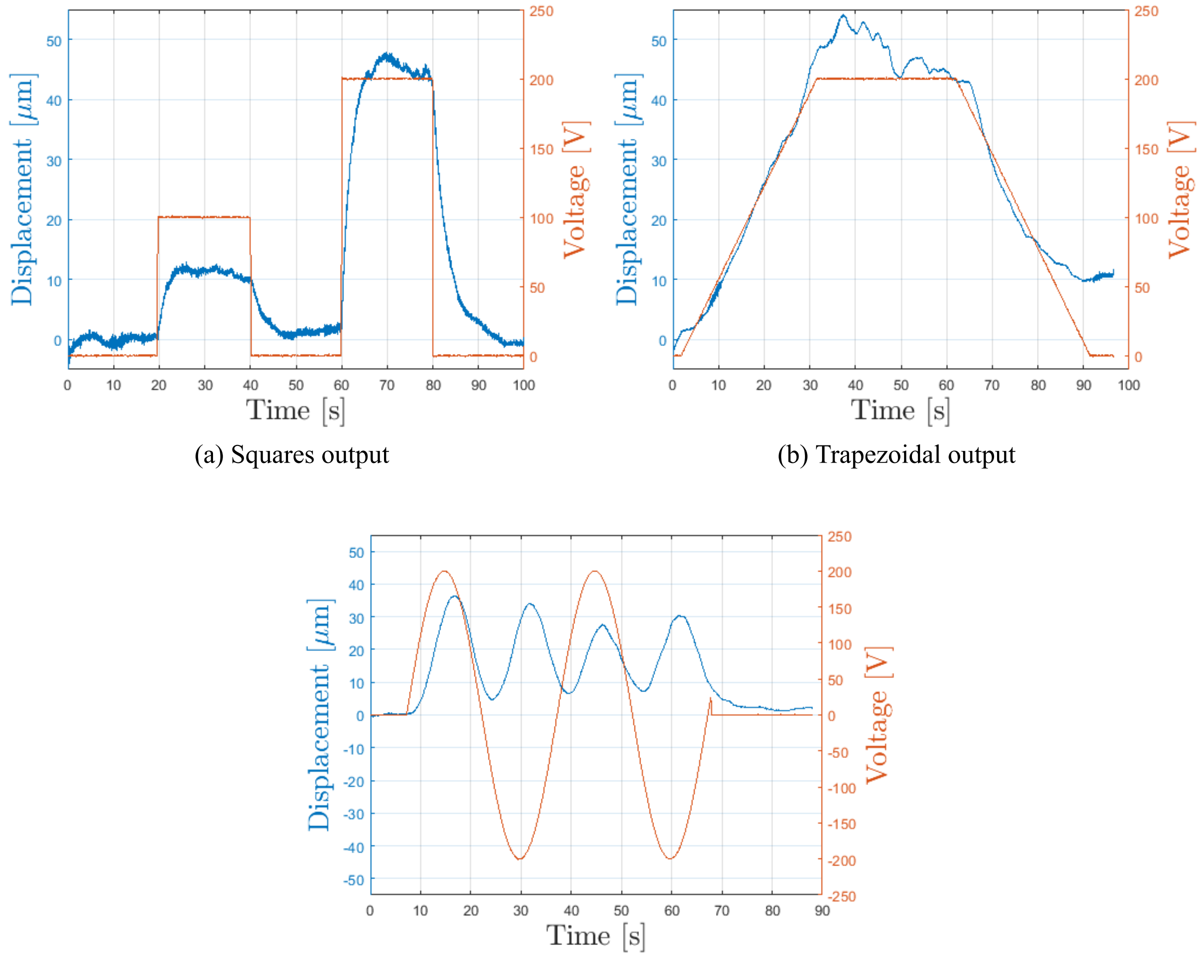

(a) Squares output

(b) Trapezoidal output

(c) Sine output

Figure 3.5: Sampled output displacement. Displacement test

Type of NN	NARX feedforward-closed loop
# HIDDEN LAYERS	1
# OUTPUT LAYERS	1
# INPUT DELAYS	3 for y ; 3 for u
# NEURONS HIDDEN	10
MINIMUM GRADIENT	$1e-11$
TRAINING METHOD	trainlm (Levenberg–Marquardt)
FUN. HIDDEN LAYER	sigmoid
FUN. OUTPUT LAYER	linear

Table 3.2: Neural network setting for displacement test

Chapter 4

Results

In this chapter, it will be analyzed the results coming from the experimental part. The results are divided into two parts following the division done in the experimental part: Force test results and Displacement test results.

4.1 Force test result

The train of the neural network, in general, didn't stop because the minimum gradient was reached but cause the number of epochs was reached. This implies that the minimum gradient was too low. In performing the training of the open-loop NN, has been computed the error between the sampled force data and the predicted one. Figure 4.1 shows the error in open loop. As was possible to see, the error was low enough to say that the trained NN was a good approximation of the real system. To define the validity of the NN in the closed-loop has been furnished as input only the signal in Figure 3.1c. What has been obtained is shown in Figure 4.3. Figure 4.2, instead, shows the error between the NN output respect the sampled force. To have a double-check of the goodness of the nonlinear model identified, the same input has been used in the linear model. Figure 4.4 shows the response of the two systems. Is easy to see that the nonlinear model better fit the real output. Moreover, to have a comparison between the two methods of identification, it has been computed the *Root Mean Square Error* of the two identifications. The value computed confirms the goodness of the nonlinear model respect the linear one, indeed:

$RMSE(e_{NN})$	0.0014
$RMSE(e_{l})$	0.0030

Table 4.1: Root Mean Square Error for identification error

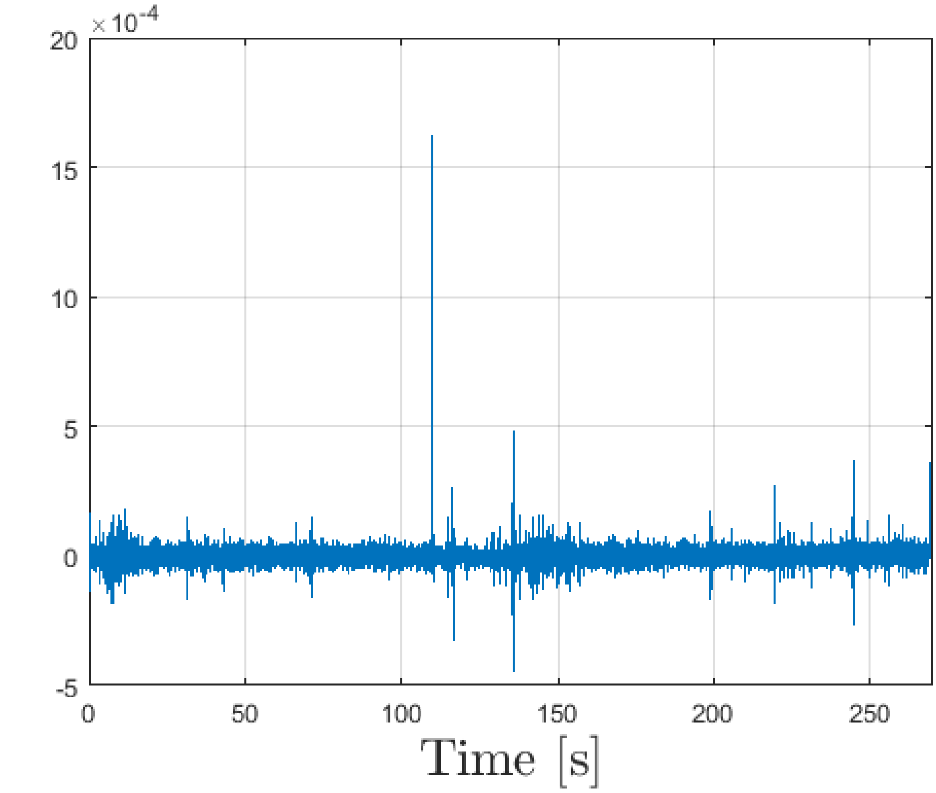

Figure 4.1: Training error of forward neural network

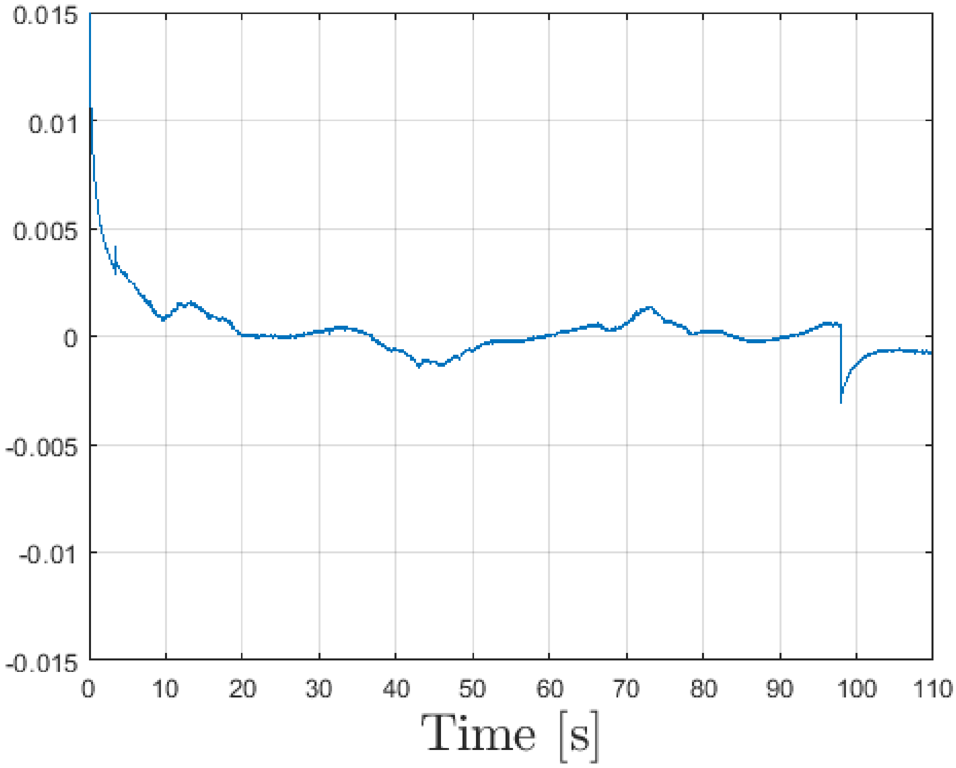

Figure 4.2: Error of closed loop neural network

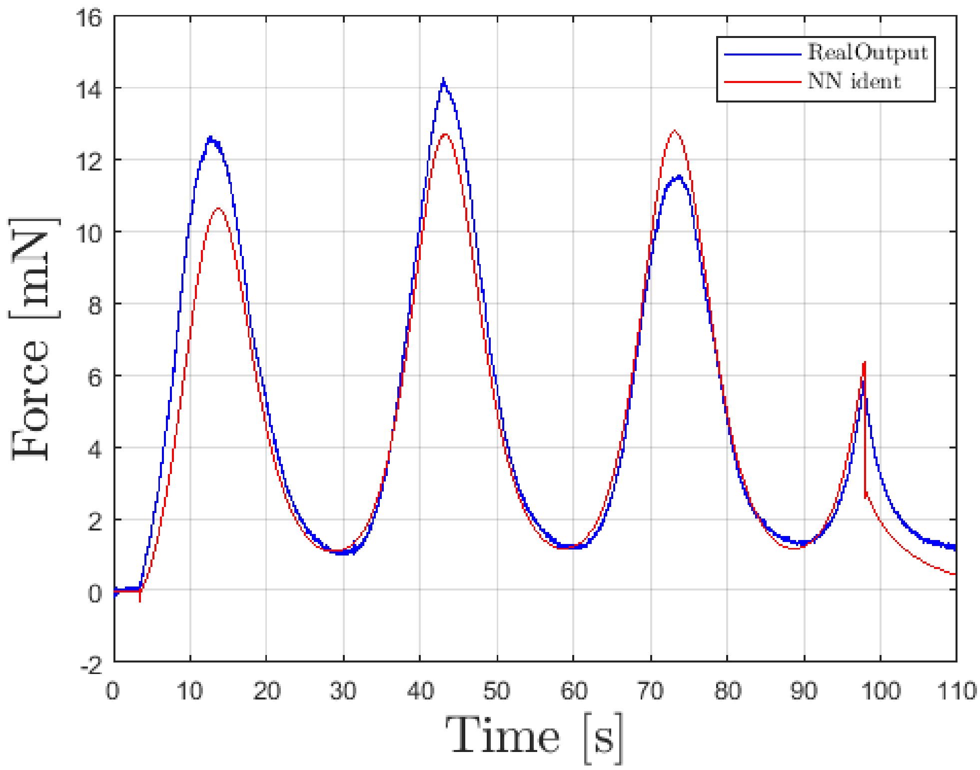

Figure 4.3: Comparison real output and neural network output

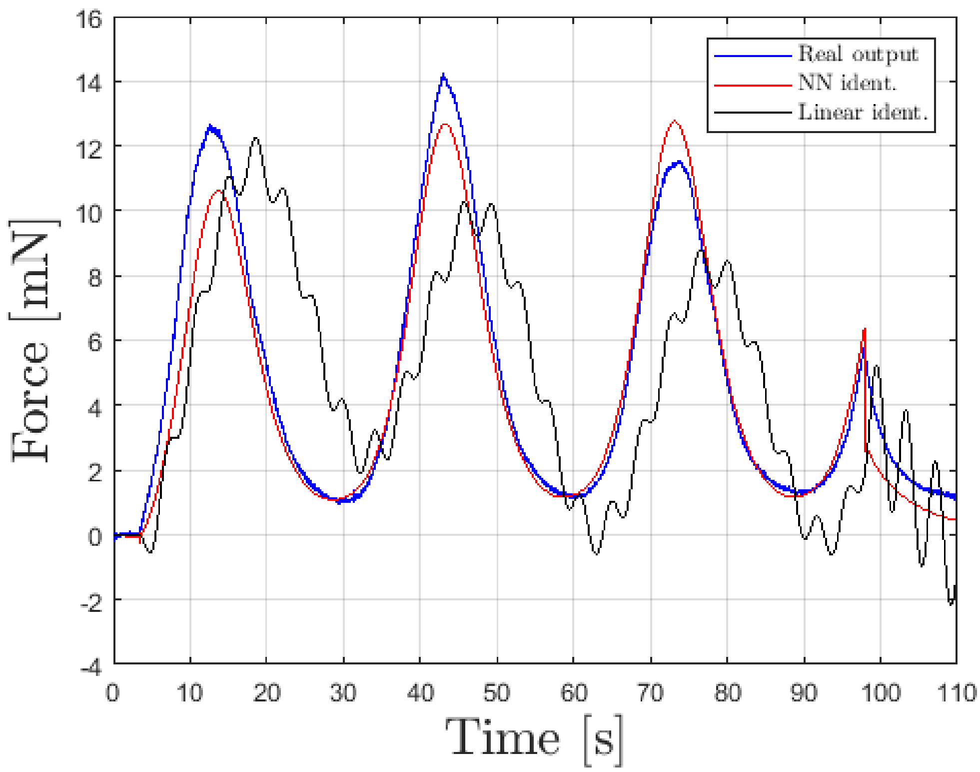

Figure 4.4: Comparison outputs of the linear system, neural network and real system

4.2 Displacement test results

The displacement test demonstrates that the bundle contracts in the vertical direction under a constant preload. As in the case of the NN for force test, also in displacement test, the NN has been trained on an open-loop network. The training error is shown in Figure 4.5. From the figure is possible to notice how the training error is low enough to say that the NN is a good approximation of the training data. To validate the NN it has been selected one of the input signals, the one shown in Figure 3.5c. Figure 4.7, shows the comparison of the sampled displacement data and the NN output prediction. During the training phase have been used a different combination of *input delays* and a different number of neurons but the best combination has been the one shown in the table 3.2. Finally has been analyzed the error between the real output and the estimated one. Figure 4.6 shows the comparison error. As in the case of the force test, the *Root Mean Square* has been computed on the comparison error. It comes out an *RMSE* of 0.0044. It has been performed also a linear identification of the system based on the same training data of the NN. The one step ahead prediction of the linear model was completely different even trying to change the configuration of poles and zeros.

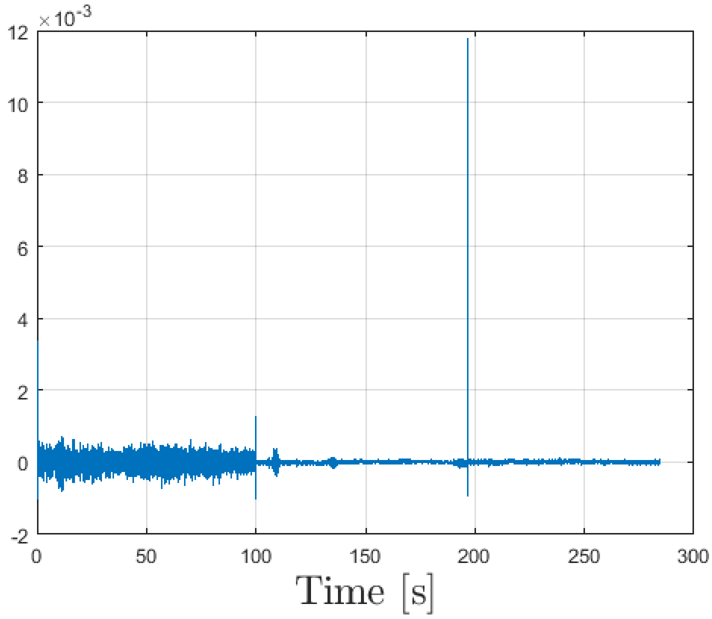

Figure 4.5: Training error of displacement test

Another point to make is related to the figures 3.5c. It is possible to notice that when the voltage inverts the polarity, the bundle had a contraction in a positive direction. So either the input is positive or negative, the bundle will move always in the same direction with the same intensity. The fact that the strain (S) is always in one direction can be explained by its quadratic dependency to the electric field. The electrostrictive law well defines this behaviour [5]:

$$S = QP^2 \tag{4.1}$$

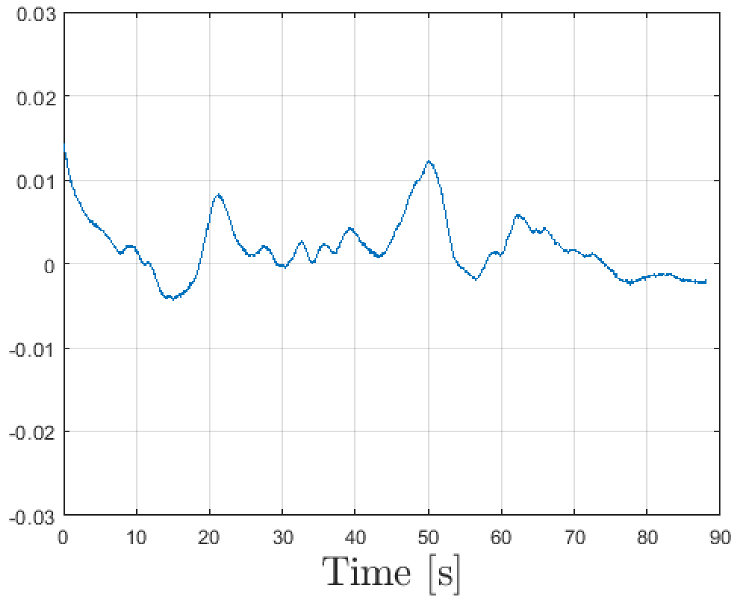

Figure 4.6: Validation error. Displacement test

where Q is the charge-related electrostrictive coefficient and P is the polarization or electric field. The electrostriction is not the only phenomena acting on the bundle, indeed as reported by [12], the behaviour of the bundle is due to different phenomena i.e. thermal, electrostrictive, electromechanical, so it is not easy to have a well defined physical model. From this reason come the needed to switch to a nonlinear black-box identification.

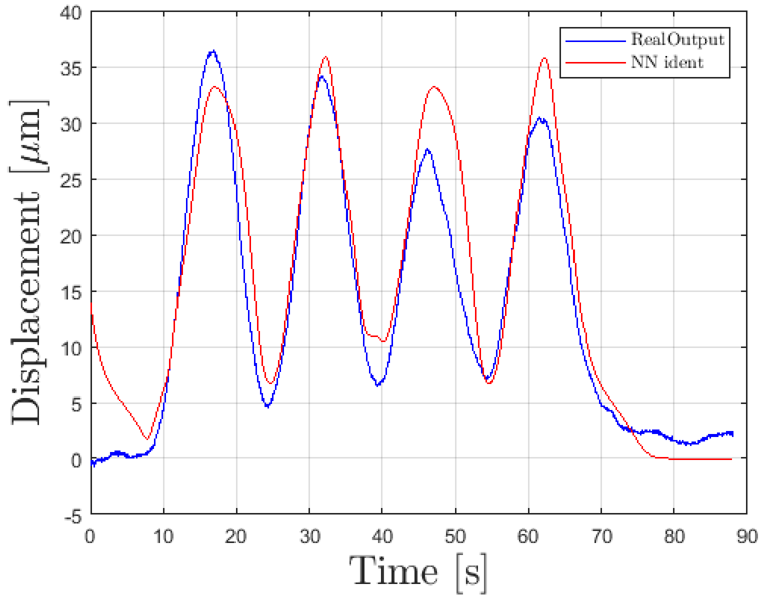

Figure 4.7: Validation data: comparison real output and NN output

Part II

APPLICATION

Application and control

In the first part of this work, it has been analyzed and defined the black-box model for the bundle of PU plus salt. As introduced in the first part the PU plus salt can be seen as an electroactive soft actuator. This second part shows a possible usage of the identified actuator: a position control and energy analysis for application of the bundle as artificial muscles have been found.

Chapter 5

Control setup

The setup used for the control part is mostly the same used for the identification part. It has been used a Raspberry pi model B 3 to perform the control unit. The output signal of the Raspberry pi is then amplified by the operational amplifier lm324n. The output is then used to drive a MOS-FET connected to the amplifier TREK MODEL 10/10B-HS thought a BNC cable. It has been used two 3D printed clamps in ABS for the position control, and a 3D printed ABS structure to show a possible application of the bundle. In the position control has been used the Logitech Hd Pro Webcam C920 camera for position tracking. A laptop it has been used for image calibration and for upload the code in the raspberry board.

Chapter 6

Experiments

6.1 Position control

From the first part it has been demonstrated that under a certain applied voltage, the bundle of PU plus salt contracts up to 40 $[\mu m]$.

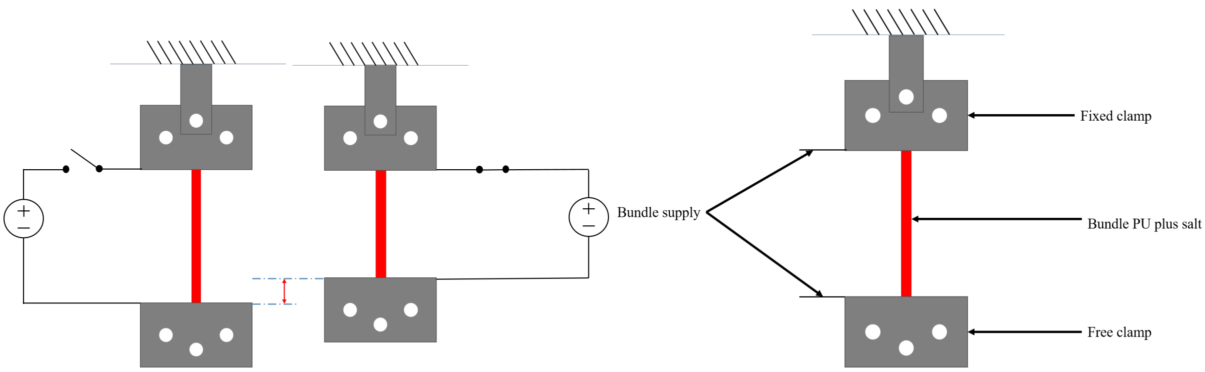

(a) PU plus salt property (b) Position control set-up

Figure 6.1: Control clamps setup

The setup for the experiment is shown in Figure 6.1b: the bundle is held on one side by a fixed clamp. The other side of the bundle is then held by another clamp free to move. The weight of the free clamp is 17.67 $[g]$. This implies that on the free side of the bundle is applied a force of 0.17 $[N]$, similar to the preload defined in the identification section. To build a suitable *control action* for the model (voltage-displacement), it has been created a *simulation* test scheme (Figure 6.2) in the Simulink environment.

A discrete PID has been selected considering a sample time of 1 $[Hz]$ and the parameters of the *proportional* K_P, *integral* K_I and *derivative* K_D action reported in table 6.1. Once the control law has been define can be exported to the electronic board Raspberry pi. The Figure 6.3 shows as the Raspberry pi has been used as a control unit for the displacement monitoring and control. Note that the camera Logitech has been connected to the raspberry board for images acquirement. The camera has been used as position tracking to have an indirect access to the

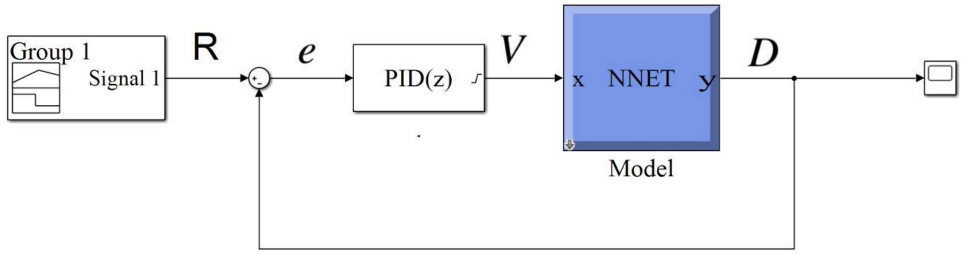

Figure 6.2: Simulation scheme

K_P	7000
K_I	300
K_D	200

Table 6.1: PID control parameters

position of the free clamp. This sensor has been used as a feedback sensor. For the actuation instead has been used a signal conditioning circuit. From the Raspberry pi GPIO 18 has been produced a *Pulse-width modulation* (PWM) wave ranging from 0 to 3.3 $[V]$. This signal is then amplified through an operational amplifier up to 5.5 $[V]$. The latter is next used to drive the gate port of MOSFET. From the MOSFET it has been obtained an output voltage of $0 - 250$ $[mV]$ then amplified by the TREK MODEL 10/10B-HS up to $0 - 250$ $[V]$.

6.1.1 Image calibration for potion control

Before to embed the control in the Raspberry and proceed in the experiment, an offline procedure for image calibration has been done. The procedure can be resumed in four steps:

- acquire the image from the camera;
- define the gain $Pixel \rightarrow mm$;
- define the reference coordinates (x_0, y_0);
- define the pixels region of interest.

The first step is the acquisition of the image with the laptop. Figure 6.4a shows Matlab reference axes $(0, 0)$ coordinates defined in the upper-left corner. Step 2 aims to convert a displacement of tracked points in mm. Each time the clamp is removed and put back, the calibration procedure has to be performed again. In defining the region of interest is worth to mention how Matlab define it. In general, the region can be defined in a different method, but the one that has been used is the “imrect”: the region is defined by a 4-element vector of the

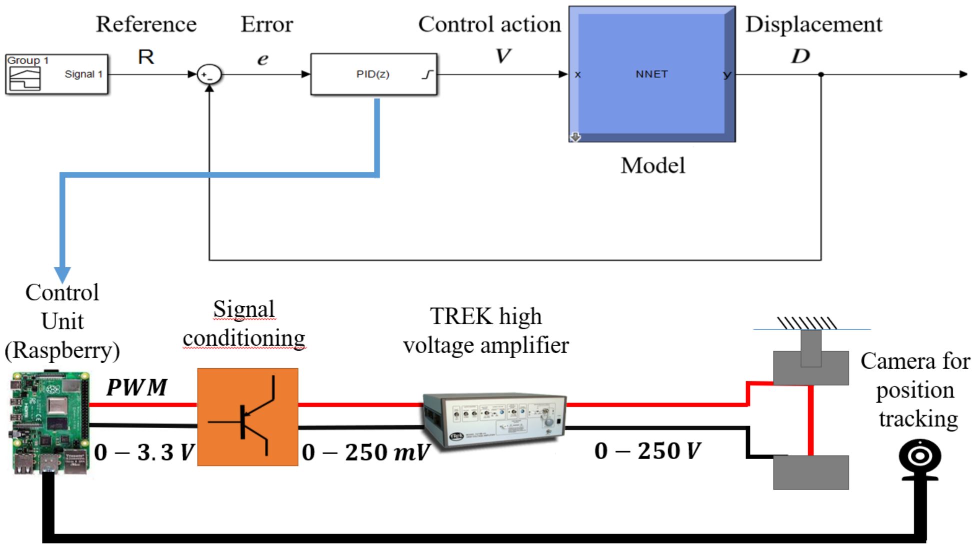

Figure 6.3: Raspberry pi setup, control law uploading

form [x_{min} y_{min} $width$ $height$]. The first two are x and y coordinates of the upper-left corner of the rectangle. Then the other two are respectively the width and the height of the rectangle. All the points are defined in pixel. Step 3 has been used to define the new references axes. The parameter obtained from the image calibration are: *initial reference*, $(x\_init\ \ y\_init)$, the *region of interest*, and *gainPx2mm*.

6.1.2 Control script

The control script has been written in the Matlab language. It has been divided into different parts. The first parts contain all the initialization instructions i.e Raspberry pi configuration (need for the upload of the code from Matlab to the Raspberry), camera initialization (needed to allow Raspberry pi to take a picture from the Logitech Hd Pro Webcam C920). Moreover have been defined also the parameters for the PWM i.e frequency, duty cycling and Raspberry GPIO. Then are insert manually the value of *initial reference*, $(x\_init\ \ y\_init)$, the *region of interest*, and *gainPx2mm* defined in the offline image calibration step. Next, it has been defined all the parameters concerning the control part i.e the control parameters (K_P , K_D, K_I), the reference and the sample time. Since the PWM function accepts only values within $[0\ 1]$, it has been defined as a linear mapping function, from the control action to PWM values.

At this point, it has been defined the core of the control part that cycles these instructions:

- it acquires a frame image;
- having in memory the region of the points to be tracked, the code gives back the coordinates of the points in frame sampled;
- the points obtained, are expressed respect the new reference, and converted in mm;
- the error between the reference and the actual position is computed;

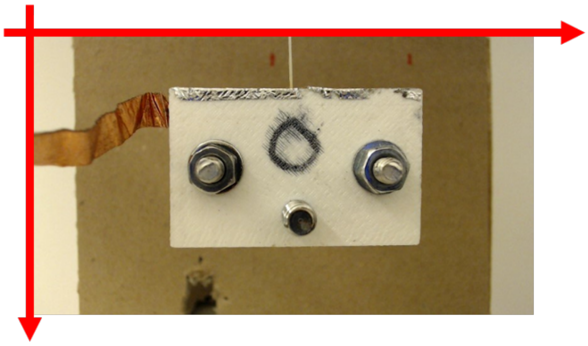

(a) Step 1: image acquiring, Matlab image reference

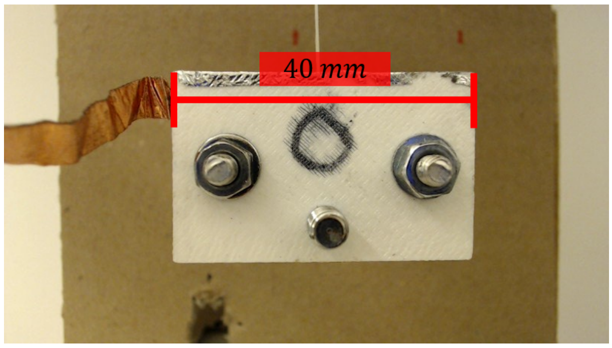

(b) Step 2: definition of the gain to convert pixels in mm.

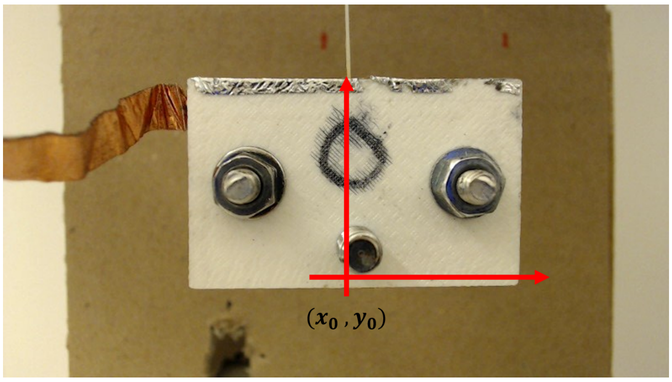

(c) Step 3: definition of the new axes reference

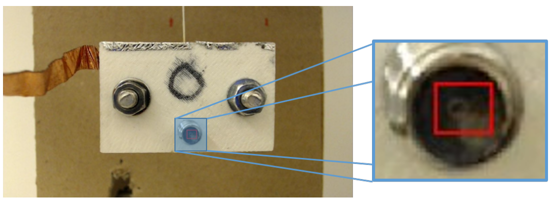

(d) Step 4: definition of the region of interest

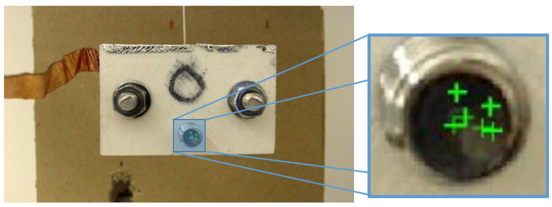

(e) Step 4: definition of the points of interest

Figure 6.4: Offline image calibration procedure

- the error is used to update the control action considering the parameters defined in the initialization part;
- the control action is then converted in PWM value and sent to the PWM GPIO.

Once the main core is finished the vector of data sampled of position, control action and error have been downloaded in the Matlab workspace.

Chapter 7

Results

In the first part, the result of the position control has been reported. It follows a possible future application of the PU plus salt as a robotic arm. The chapter finishes with an energy analysis of the bundle of PU plus salt.

7.1 Position control result

This section collects the results obtained from the clamp position control. As explained in the experiment part, the position control has been used to test the identified model of the bundle of PU plus salt. As said, first has been defined as a simulation in Matlab Simulink and then, the controller has been translated in Matlab code for Raspberry pi. It has been decided to control the position of the clamp attached to the bundle, specifically it has been asked to the controller to follow a step reference of $40\ [\mu m]$ for the duration of $20\ [s]$. Figure 7.1, shows the comparison

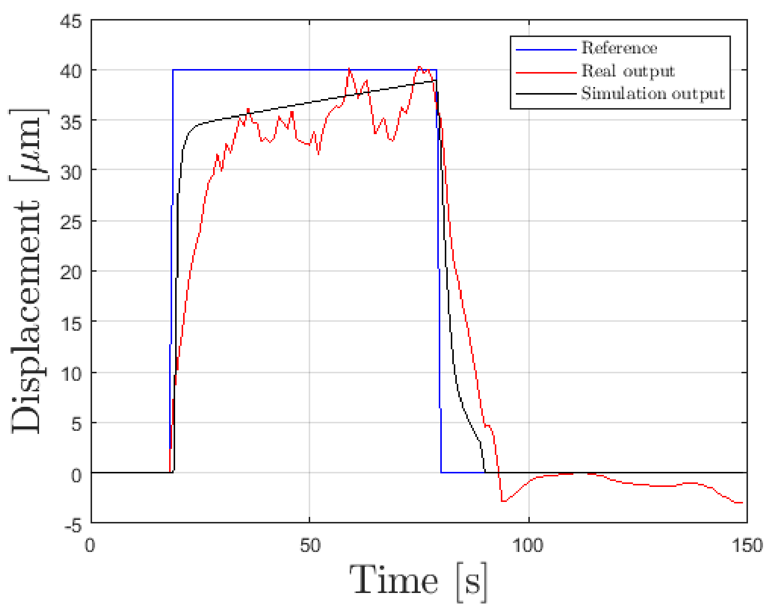

Figure 7.1: Comparison reference and outputs

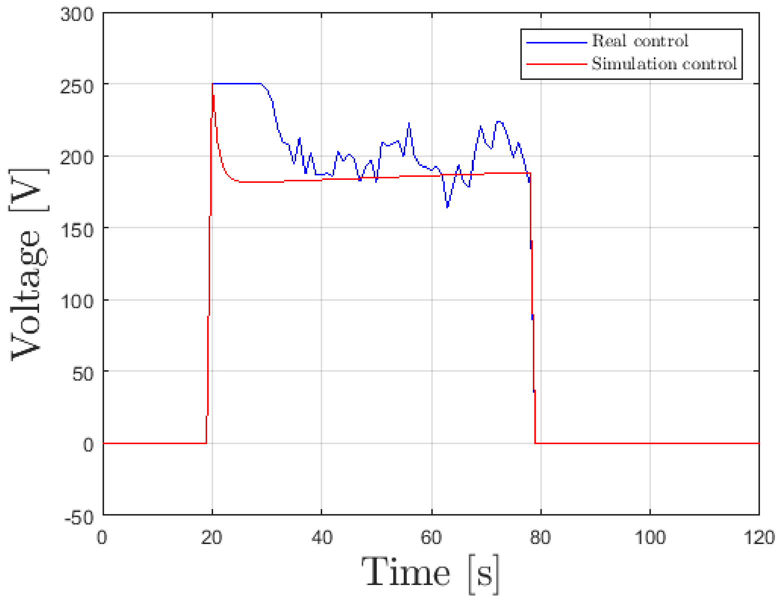

Figure 7.2: Comparison control actions

of the reference with the output of the experiment and simulation. It is possible to notice how the experimental output and the simulation are not overlapped: this can be explained by the noise due to the camera. Indeed, in the experimental output, the camera is used as a position sensor. To speed up the control action, it has been decided to reduce the resolution of the image acquired for position tracking. Doing so, a noisy position output come out and as consequence also the control action as been affected as shown in Figure 7.2.

7.2 Future application

During the work done, it has been thought a possible application for the polyurethane-based actuator: a robotic arm. Indeed, has been thought to use the actuator as a small artificial muscle adopted to move a small copper-based arm. Figure 7.3 shows the 3D printed structure. It is possible to notice that the copper tape has been added in the fulcrum of the arm. Moreover, the arm itself has been made by copper such that one side of the bundle is connected to the positive pole of the power supply. The other side of the bundle has been connected to the negative pole of the power supply through a copper tape. Tt has been performed a test applying a voltage of $300\ [V]$ to the two sides of the bundle. While the step input signal it has been applied, a video has been recorded. A the end of the experiments the tracking position has been done. Starting from the video has been taken the first frame and has been performed the same image calibration procedure seen in the *Image calibration* section. Once the *new reference*, *region of interest*, and *gainPx2mm* has been defined, a Matlab script has been executed. The procedure has been done in the same way as the *position control* but with some modification. First, the image has been acquired from the video, taking one frame per iteration. Then have been identified the points of

(a) Arm setup without bundle

(b) Arm setup with bundle

Figure 7.3: Arm setup

interest and has been extracted their coordinates. Since the points identified are more than one, it has been formed either for the x coordinate and for y the average among the coordinates of the points. Once the coordinates have been found, the pixel coordinates are expressed respect to the new reference axes. Having the position of the point respect to the axes, it has been computed the angle. Figures 7.4 hows how the angle had changes in time.

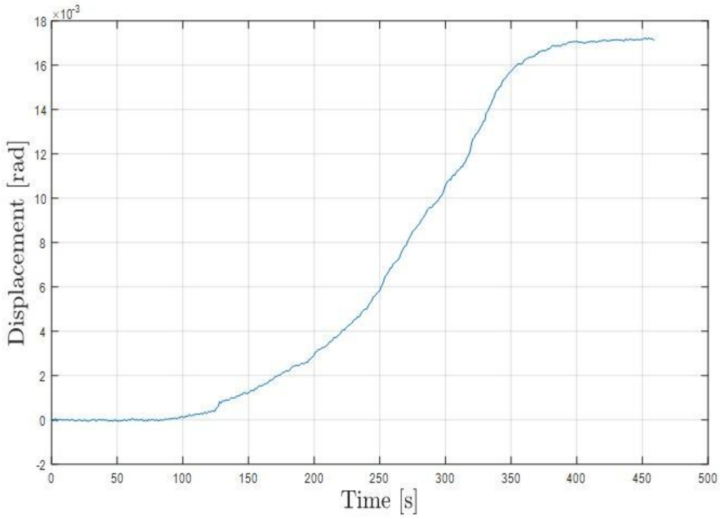

Figure 7.4: Arm displacement with 300 V input

7.3 Energy analysis

To show the performance of the bundle, and energy analysis has been performed. In particular, the electric power consumption and the force produced with respect to the weight of the material has been compared with the performance of a DC linear motor (LINMOT PO1-23x80, `https://linmot.com/`).

From the technical data-sheet of the motor is possible to evaluate the consumption of electric power to produce the maximum amount of force. The PU-based soft actuator, is able to produce a value of force F_{tot} given:

$$F_{tot} = W \cdot 9.8 + F \tag{7.1}$$

where W are the weight of the free clamp expressed in N, F is the contraction force of the specimen. The weight of the free clamp converted in N is comparable to the applied preload in the electromechanical characterization. In this way, it is possible to reasonably use as reference the contraction force values obtained during the electromechanical characterization. The dissipated electric power P_{el} of the soft actuator is:

$$P_{el} = VI \tag{7.2}$$

For the comparison, it is assumed to realize an actuator with multiple bundles in parallel. The bundles contract in the same direction with the same force and the electric current flowing in the samples is the same for every bundle. It is possible to calculate the amount of total weight W_{tot} of the PU, which is required to produce the same amount of force generated by the linear motor with a simple proportion, knowing the force produced by the single bundle (F_{tot}) expressed in kg, its weight and the force generated by the motor expressed in kg. If the bundles are connected in parallel, it is possible to calculate the number n of bundles necessary to produce the force generated by the motor, i.e.:

$$n = \frac{W_{tot}}{W_{bundle}} \tag{7.3}$$

where W_{bundle} is the weight of the single bundle. Moreover the total power consumption is given by:

$$P_{total} = nP_{el} \tag{7.4}$$

The comparison of the energy analysis is summarized in Table 7.1. The values of the current, relatives to the bundle, used for the analysis have been evaluated through the high-voltage amplifier, and are referred to the maximum applied voltage of the test of position control ($250\ [V]$), that led to a peak current value of $1.8\ [mA]$.

	Weight (g)	**Adsorbed Power (W)**	**Max Force (kg)**
Motor	265	280	4.486
Bundle	$\sim$0.007	$\sim$0.45	$\sim$0.0234
Parallel bundles	$\sim$1.34	$\sim$86	$\sim$4.486

Table 7.1: Comparison of performance between a DC motor, a single bundle and a parallel connection of several bundles.

Conclusion

This work focuses on the analysis and utilization of an electroactive soft actuator, made of polyurethane-based nanofibers. On a bundle made by aligned nanofibers of polyurethane and a salt has been performed several electromechanical test using the machine Instron™ static ElectroPlus E1000 equipped with the Instron™ static load cell 2530-5N. The data sampled of voltage, force, and displacement have been then used for nonlinear system identification of the soft actuator bundle. It has been noticed the quadratic dependency between voltage and displacement/force. A possible application of the soft actuator has been designed. To conclude it has been compared the soft actuator with a linear DC motor: it has been shown how a collection of parallel bundles of PU plus salt absorbs less electric energy respect to linear DC motor, based on similar maximum output force. Thanks to the low-cost production, to the better efficiency, to the low weight-bundle/weight-lifted, the polyurethane-based soft actuator could be used to replace electric motors.

Bibliography

[1] M Roussel et al. “Electromechanical study of polyurethane films withcarbon black nanoparticles for MEMS actuators”. In: *J. Micromech. Microeng.* 24 (2014).

[2] Théo Calais and Pablo Valdivia y Alvarado. “Advanced functional materials for soft robotics: tuning physicochemical properties beyond rigidity control”. In: *Multifunct. Mater* 2 (2019).

[3] Jong Yuh Cherng et al. “Polyurethane-based drug delivery systems”. In: *International Journal of Pharmaceutics* 450.1 (2013), pp. 145–162. ISSN: 0378-5173. DOI: `https://doi.org/10.1016/j.ijpharm.2013.04.063`. URL: `http://www.sciencedirect.com/science/article/pii/S0378517313003645`.

[4] Notarstefano Giuseppe. *Note of Distributed control system*. 2019.

[5] Kwan Chi Kao. *Dielectric Phenomena in Solids*. Vol. 1. Elsevier Academic Press, 2014, pp. 49–50.

[6] Frederick Largilliere et al. “Real-time Control of Soft-Robots using Asynchronous Finite Element Modeling”. In: *ICRA* (2015), p. 6.

[7] Oliver Nelles. *Nonlinear System Identification, From Classical Approaches to Neural Networks and Fuzzy Models*. Vol. 1. Springer, 2001, pp. 49–50.

[8] *Neural Network Toolbox User’s Guide*. October 2004.

[9] Ohmukai et al. “Electrode Effects on Polyurethane Soft Actuator”. In: *World Journal of Engineering and Technology* 05 (Jan. 2017), pp. 520–525. DOI: `10.4236/wjet.2017.53044`.

[10] Seeram Ramakrishna. *An Introduction to Electrospinning and Nanofibers*. World Scientific Publishing, 2005.

[11] Daniela Rus and Michael T. Tolley. “Design, fabrication and control of soft robots”. In: *Nature* 521 (2015), pp. 467–475.

[12] Hiroaki Sakamoto et al. “Fabrication and Characterization of FE/Polyurethane Nanofiber Actuator Prepared by Electrospinning”. In: *Journal of Fiber Science and Technology* 73 (6 2017), pp. 135–138.

[13] Jonas Sjöberg et al. "Nonlinear black-box modeling in system identification: a unified overview". In: *Automatica* 31.12 (1995). Trends in System Identification, pp. 1691–1724. ISSN: 0005-1098. DOI: https://doi.org/10.1016/0005-1098(95)00120-8. URL: http://www.sciencedirect.com/science/article/pii/0005109895001208.

[14] *System Identification Toolbox™ Getting Started Guide*. October 2004.

[15] Maxime Thieffry et al. "Dynamic control of soft robots". In: *IFAC World Congress* (2017).

[16] S. Wittmeier et al. "Toward anthropomimetic robotics: development, simulation, and control of a musculoskeletal torso". In: *Artificial Life* 19 (2013), pp. 171–193.

Paper

In the following, it has been presented the paper extracted from this master thesis. The paper has been submitted to the *International Conference on Intelligent Robots and Systems* (IROS). The work done has been developed together with R. D'Anniballe and R. Carloni from the Faculty of Science and Engineering, University of Groningen, The Netherlands. {r.danniballe,r.carloni}@rug.nl

A Polyurethane-based Soft Actuator: Fabrication, Modeling, and Control

Giovanni Paoletta[1], Riccardo D'Anniballe[2], and Raffaella Carloni[2]

Abstract— **This paper presents the analysis and utilization of an electroactive soft actuator, made of polyurethane-based nanofibers. A mat of aligned nanofibers of polyurethane and a salt has been fabricated through an electrospinning process and, subsequently, has been rolled up to form a bundle of aligned nanofibers. From the same bundle, three specimen have been obtained, i.e., three polyurethane-based soft actuators. Several electromechanical tests on one specimen have been performed to evaluate the forces and the displacements generated by the soft actuator when an electrical input is applied. The data generated during the electromechanical tests have been used in a neural network to derive the non-linear model of the soft actuator. Subsequently, the model has been used to design a position control scheme, which has been tested on a second specimen. The performances of the soft actuator have been compared to a DC linear motor with similar maximum output force. Finally, to validate the contraction capabilities of the soft actuator, a third specimen has been used to actuate a robotic arm.**

I. Introduction

Polyurethane (PU) is a versatile thermoplastic polymer with good mechanical property, such as flexibility and low density. PU is also bio-compatible, biodegradable and, therefore, suitable for medical applications [1]. PU has been also used as soft actuator. In [2], the bending characteristics of a film of a polyurethane elastomer with different metal electrodes has been analized. Iron chloride has been electrospun with a polyurethane matrix in [3] to realize a conductive nanofibrous actuator. In [4], carbon powders have been used as conductive filler in a polyurethane film to realize microelectromechanical actuators.

Soft actuators and soft robots requires new approaches for dynamic modeling and control [5]. Classical kinematic and dynamic modeling techniques cannot be directly used in soft robotics because soft robots are highly non-linear systems, and the sensitivity of the materials used therein can cause a change in the dynamics of the system. Several novel control approaches can be found in the literature: in [6] and [7], finite element methods are use to derive a dynamical model of the soft robots, in [8] different control approaches inspired by classical control theory, machine learning, and neuroscience have been evaluated for the control of a cable-driven robot.

This work was funded by the European Commission's Horizon 2020 Programme as part of the project MAGNIFY under grant no. 801378.

[1]Giovanni Paoletta is with the Faculty of Engineering, University of Bologna, Italy. g.paoletta@studio.unibo.it (This work was done while G. Paoletta was with the Faculty of Science and Engineering, University of Groningen, The Netherlands.)

[2]R. D'Anniballe and R. Carloni are with the Faculty of Science and Engineering, University of Groningen, The Netherlands. {r.danniballe,r.carloni}@rug.nl

This paper focuses on a soft actuator, which consists of a bundle of aligned nanofibers of polyurethane and a salt that acts as conductive filling. The aligned nanofibers have been realized through an electrospinning process, i.e., an efficient technique to produce small-diameter (from nanometer to micrometer scale) polymeric fibers oriented in the fiber length direction. Nanofibers are characterized by high porosity and high surface-volume ratio, and their physicochemical properties can affect their actuation driving process [9].

In this paper, the soft actuator is analyzed and electromechanically characterized to evaluate the forces and the displacements generated when an electric field is applied. The experimental data are used to derive a non-linear dynamic model, which has been identified by using an artificial neural network. The obtained model has been used to design a position control scheme for the soft actuator and for a robotic arm, in which the soft actuator is implemented. The performances of the soft actuator have been compared to a DC linear motor in terms of dissipated electrical power and produced mechanical power.

The remainder of the paper is organized as follows. Section II presents the fabrication of a PU-based soft actuator. Section III presents the experimental set-up to measure the forces and displacements produced by the soft actuator when an electric field is applied. In Section IV, the dynamic model of the soft actuator is derived by using a non-linear system identification method based on an artificial neural network. In Section V the model is used to design a control system for the position control of the soft actuator. In Section VI a robotic arm that exploits the soft actuator is realized and tested. Finally, concluding remarks are drawn in Section VII.

II. Fabrication of the Polyurethane-based Soft Actuator

This Section presents the fabrication of the nanofibrous PU-based soft actuator, as sketched in Figure 1.

The soft actuator consists of a bundle of aligned nanofibers of PU[1] and a salt[2]. The aligned nanofibers have been fabricated by an electrospinning process [10], [11], in which the polymeric solution of PU and the salt is stretched in a high electrostatic field. Specifically, the electrospinning machine consists of a syringe with a thin metallic needle, loaded with the solution and a solvent, a syringe pump to control the flow rate, and a metallic rotating collector positioned at a certain distance. The needle is linked to the positive

[1]Poly[4,4-methylenebis(phenylisocyanate)-alt-1,4-butanediol/di(propyleneglycol)/polycaprolactone].

[2]Tetrabutylammonium hexafluorophosphate.

of a high-voltage DC power supply, while the collector is grounded. The high electrostatic field between the needle and the collector causes the solution to flow out of the needle and to form a mat of aligned nanofibers on the collector. The nanofibrous mat has been rolled up to form a bundle of aligned PU nanofibers with the salt that acts as a conductive filler. Note that the PU is an insulating material, but the bundle becomes conductive because of the salt added during electrospinning. Therefore, the bundle is a soft actuator that, when a voltage is applied at its extremities, contracts in the axial direction and shows an axial displacement.

The obtained bundle has been cut to realize three specimen, i.e., three soft actuators. The dimensions of the three actuator are the following: 40 mm in length, ≈ 0.6 mm in diameter, ≈ 7 mg in weight. Of the three specimens, one has been used for the electromechanical characterization and for the derivation of the dynamic model (see Sections III and IV, respectively). A second specimen has been used to validate the model and to test a position control scheme (see Section V). The third specimen has been used to actuate a robotic arm and to show the utilization of the soft actuator (see Section VI).

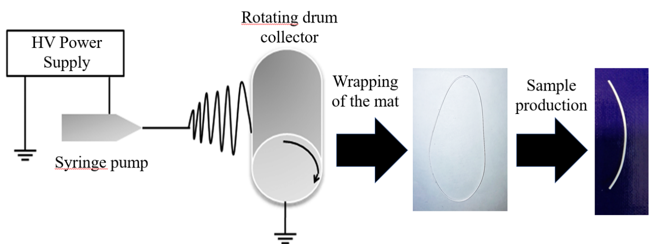

Fig. 1: Fabrication steps of the PU-based soft actuator.

III. Electromechanical Characterization of the Polyurethane-Based Soft Actuator

This Section presents the electromechanical characterization of the PU-based soft actuator. The characterization consists in measuring the axial displacement and the axial contraction force of the soft actuator when a voltage is applied at its extremities.

A. Measurement Set-up

The electromechanical characterization has been performed with the test instrument Instron™ ElectroPuls E1000 (`www.instron.us`), equipped with the Instron™ static load cell 2530-5N, which has a capacity of ± 5 N and a sensitivity of 1.6 mV/V to 2.4 mV/V at static rating. The measurement set-up is depicted in Figure 2.

The specimen is placed inside the Instron testing instrument and clamped with two grips, which have been 3D-printed in ABS material. The surfaces of the grips are covered with copper tape and connected to a TREK 10/10B-HS high-voltage amplifier (`www.trekinc.com`) through crocodile plugs, in order to apply a voltage to the specimen. The high-voltage generator is controlled by a RIGOL DG1022 input waveform generator (`www.rigolna.com`).

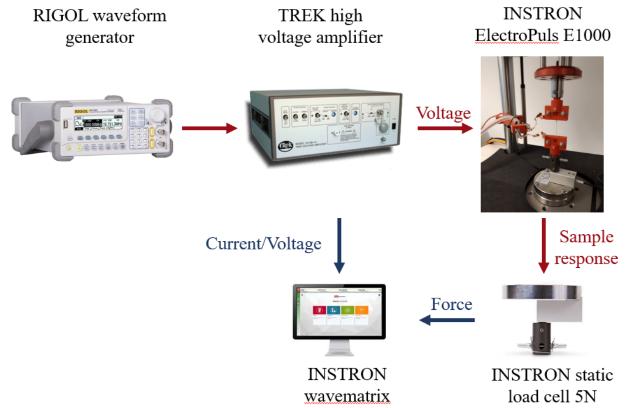

Fig. 2: Measurement set-up for the electromechanical characterization of the soft actuator: the Instron ElectroPuls E1000 receives voltages as inputs and registers the response of the specimen (either a force or a displacement). The Instron wavematrix software collects the generated data.

The Instron test instrument is either controlled to maintain a fixed displacement (the extremities of the bundle are kept at a constant distance) to measure the axial contraction force, or to maintain a fixed force (the force at the bundle is kept constant) to measure the axial displacement.

The data are collected at a sampling frequency of 1 KHz, by using two strain channels connected to the Instron test instrument, and analyzed in a desktop PC through the Instron™ Wavematrix Software. The two strain channels are used to record the displacement or the force and the current that flows through the specimen when the voltage is applied.

B. Specimen Preparation

To enhance the conductivity of the soft actuator, the specimen is prepared as follows:

- The specimen is fully immersed for 30 s in propylene carbonate (PC) solvent.
- The specimen is dried in filter paper to avoid the swelling of the nanofibers and to prevent the leakage of salt from the bundle.
- Before starting with the measures, the specimen is inserted in the 3D printed ABS clamps with a preload of 0.2 N. This value has been chosen to allow the complete relaxation of the material, after the contraction caused by the application of a voltage.
- After the specimen has been mounted on the measurement set-up, a time of 10 minutes is waited to ensure the stabilization of the specimen after the application of the preload.

C. Experimental Results: Axial Displacement

The axial displacement has been measured by performing a force control on the Instron test instrument. The instrument maintains the preload of 0.2 N on the specimen, and the displacement, produced by the nanofibrous bundle upon stimulation with high-voltages, has been measured. Three different input voltages have been applied to the specimen:

- Two square voltage inputs, i.e., 100 and 200 V.

- A trapezoidal voltage input with an amplitude of 200 V and a total period of 30 s.
- A sinusoidal voltage input with period of 30 s and an amplitude of 200 V.

The measurement are shown in Figure 3. It can be noted that the axial displacement is always positive, i.e., the specimen shows a contraction upon electrical stimulation, confirming that the bundle is electrostrictive, i.e., there is a quadratic dependency between the input (the voltage) and the output (the displacement), i.e., $S = QP^2$, where S is the material strain, Q the electrostrictive coefficient, and P the electric polarization. Other effects, such as electrothermal flows and electrostatic forces, are also present but have not been characterized.

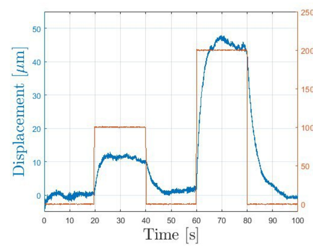

(a) Axial displacement with square voltage inputs.

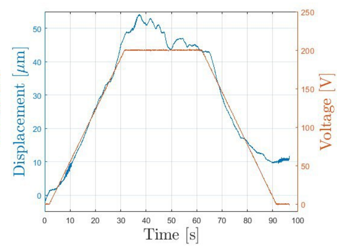

(b) Axial displacement with a trapezoidal voltage input.

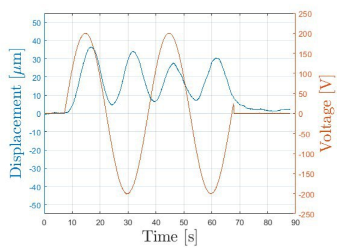

(c) Axial displacement with a sinusoidal voltage input.

Fig. 3: Axial displacements with different input voltages.

D. Experimental Results: Contraction Force

The axial force, i.e., the contraction force, has been measured by performing a displacement control on the Instron test instrument. The instrument maintains a constant distance between the grips, on which the specimen is fixed, and the contraction force, produced by the nanofibrous bundle upon stimulation with high-voltages, has been measured. Three different input voltages have been applied to the specimen:

- Two square voltage inputs, i.e., 100 and 200 V.
- A trapezoidal voltage input with an amplitude of 300 V and a total period of 30 s.
- A sinusoidal voltage input with period of 30 s, an amplitude of 250 V, and a 125 V bias.

In this tests, the negative voltage values have been excluded from the inputs, because of the quadratic dependency of the axial displacement, as reported in Section III-C.

The measurements are shown in Figure 4. It can be noted that, with increasing applied voltages, the soft actuator can generate a contraction force from several mN up to 35 mN.

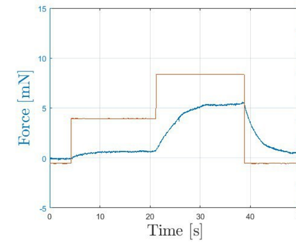

(a) Contraction force with square voltage inputs.

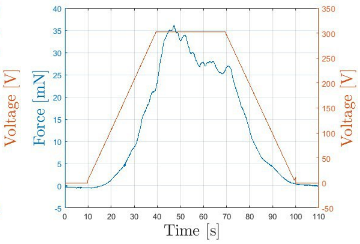

(b) Contraction force with a trapezoidal voltage input.

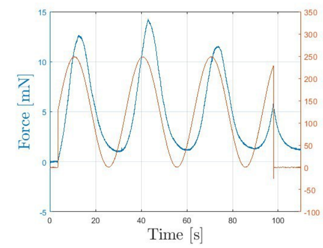

(c) Contraction force with a sinusoidal voltage input.

Fig. 4: Contraction forces with different input voltages.

IV. Dynamic model of the polyurethane-based soft-actuator

This Section presents the derivation of a non-liner dynamic model of the PU-based soft actuator.

The overlapping of different physical effects, which influence the behaviour of the specimen, are the main reason to derive the model of the soft actuator with a non-linear identification method [12]. The system identification method is preferred when the physics of the system is too complex to be described just by physical insight. The system can be analyzed as a black box model, so both the model and the parameters are determinate on experimental data. The simplest linear discrete-time input/ouput model is the autoregressive with exogenous input (ARX) or equation error model [13]:

$$\hat{y}(k) = b_1 u(k-1) + \ldots + b_m u(k-m) - a_1 y(k-1) - \cdots \\ \cdots - a_m y(k-m) \tag{1}$$

where $\hat{y}(k)$ is the predicted output (force or displacement), $u(k-1), \cdots, u(k-m)$ and $y(k-1), \cdots, y(k-m)$ are the input regressors, a_i and b_i are linear parameters.

This model can be extended to a NARX (non-linear ARX) model by replacing the linear relationship in Equation 1 with some (unknown) nonlinear function $f(\cdot)$, i.e.:

$$\hat{y}(k) = f\big(u(k-1), \ldots, u(k-m), y(k-1), \ldots, y(k-m)\big) \tag{2}$$

A comparison between the identification of linear and non-linear input/output models shows that the problem of estimating the parameters a_i and b_i extends to the problem of approximating the function $f(\cdot)$.

In this work, the function $f(\cdot)$ is an artificial neural network and, specifically, a Multilayer Perceptron Network (MLP) with a sigmoid activation function. The output of the MLP is the combination of the perceptron outputs and can be computed as follows:

$$\hat{y} = \sum_{i=0}^{M} w_i \Phi_i \left(\sum_{j=0}^{p} w_{ij} u_j \right) \quad \text{with } \Phi_0(\cdot) = 1 \text{ and } u_0 = 1 \tag{3}$$

where w_i are the weights output layer and w_{ij} are the weights of the hidden layer. The optimization technique is a gradient-based Levenberg-Marquardt.

Table I shows the main settings of the MLP used in this work and implemented in the Deep Learning Toolbox of MATLAB (Mathworks).

TABLE I: Setting for the MLP.

Type Neural Network	NARX feedforward-closed loop
# HIDDEN LAYERS	1
# OUTPUT LAYERS	1
# INPUT DELAYS	6 for y; 6 for u
# NEURONS HIDDEN	10
MINIMUM GRADIENT	$1e^{-11}$
TRAINING METHOD	trainlm (LevenbergMarquardt)
FUN. HIDDEN LAYER	sigmoid
FUN. OUTPUT LAYER	linear

A. Experimental results: Contraction Force

The identification of the non-linear model has been done by using the data collected as described in Section III-D. The validation has been done by using the sinusoidal data.

From the sampled data, a linear identification of the system has also been done with the MATLAB System Identification Toolbox. Figure 5 shows the comparison between the experimental data, the linear identification with a transfer-function with 5 zeros and 7 poles, and the non-linear identification with the MLP.

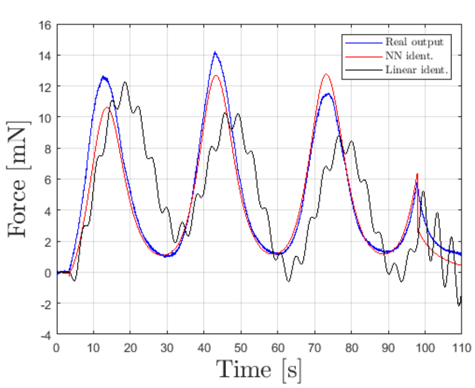

Fig. 5: Identification of the axial force of the specimen.

The error of the non-linear identification on the validation datas has a Root Mean Square Error (RMSE) of 0.0014. The error of the linear identification instead has a RMSE of 0.0033. It can be noted that the non-linear identification fits better the real behaviour of the system. For this reason, the linear identification has not been considered further.

B. Experimental results: Axial Displacement

The results of the non-linear identification are shown in Figure 6. The error between the experimental data and the non-linear identification has a RMSE of 0.0041.

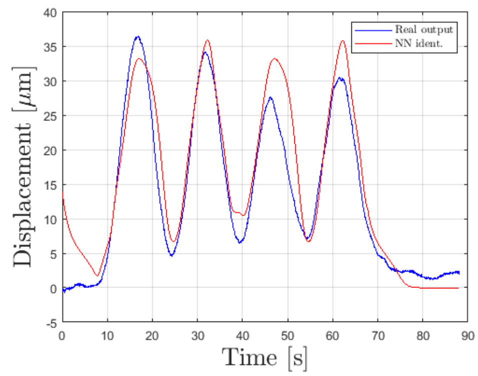

Fig. 6: Identification of the axial displacement of the specimen.

V. CONTROL OF THE POLYURETHANE-BASED SOFT ACTUATOR

This Section presents a position control scheme that has been designed on the non-linear model of the PU-based soft actuator, as identified in Section IV.

The identified model has been used in the simulation environment MATLAB/SIMULINK, as depicted in Figure 7.

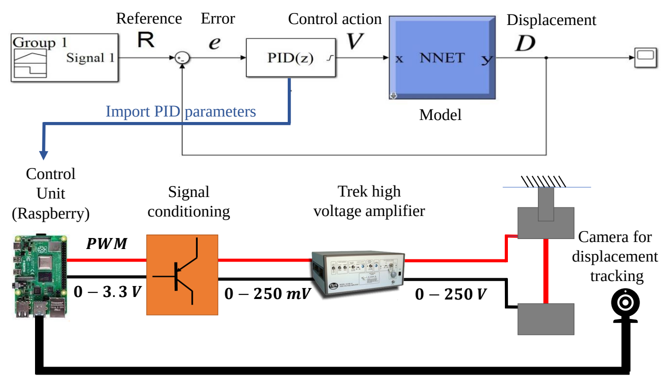

Fig. 7: The position control scheme for changing the axial displacement of the soft actuator.

A PID position control has been designed with the following parameters, i.e., $K_p = 7000$, $K_d = 200$, and $K_i = 300$. The MATLAB/SIMULINK scheme has been imported in a Raspberry PI 3 (Model B) control unit. The PWM signal of the Raspberry is fed into a signal conditioning circuit, made by a MOSFET, to obtain an analog signal in the mV range. Through a BNC adapter, the circuit has been connected to the TREK high-voltage amplifier, which amplifies the signal in the V range by means of a fixed gain of 1000. The axial displacement of the bundle is registered and sampled with a camera connected to the Raspberry unit.

The experimental set-up is reported in Figure 8, where the specimen is clamped at the top, while the bottom extremity is attached to a grip but it is free to move. When a voltage is applied, the specimen contract and the axial displacement changes.

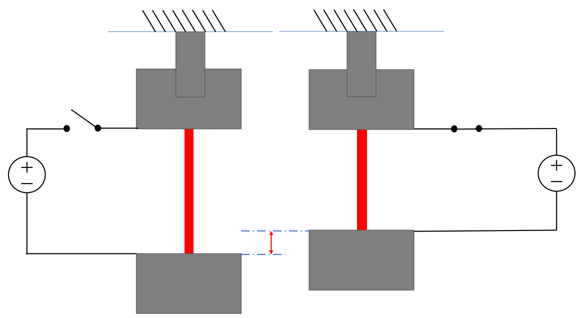

Fig. 8: The soft actuator (in red) is clamped at the top, while the bottom is attached to a grip but it is free to move. When a voltage is applied, the soft actuator contracts and the bottom grip is lifted.

Before applying the voltage and, therefore, before starting the position control, an offline calibration of the image is performed, which consists of the following steps:

a) Acquisition of the image from the camera.
b) Definition of the conversion from pixel to mm to define the measured reference of the image.
c) Definition of the reference coordinates.
d) Definition of the pixels region of interest to track.

These steps are summarized in Figure 9. Figure 10 shows the simulated control action and the real control action. Figure 11 shows the simulated and the real displacement.

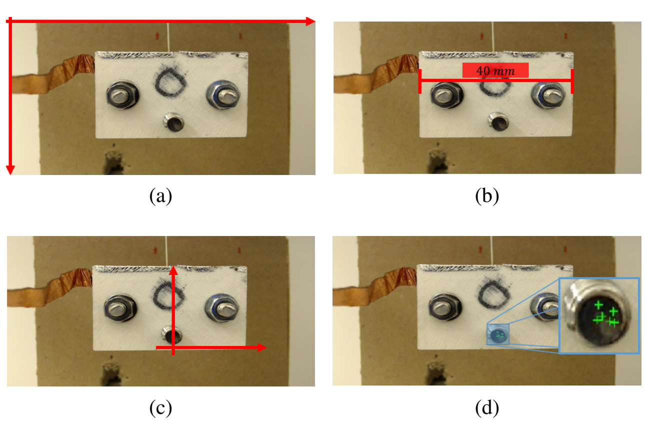

Fig. 9: Offline calibration of the camera for the recording of the displacement.

A. Energy Analysis

To show the performance of the bundle, an energy analysis has been performed. In particular, the electric power con-

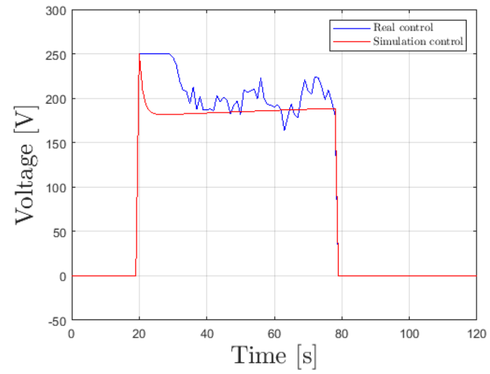

Fig. 10: Simulated and real control action.

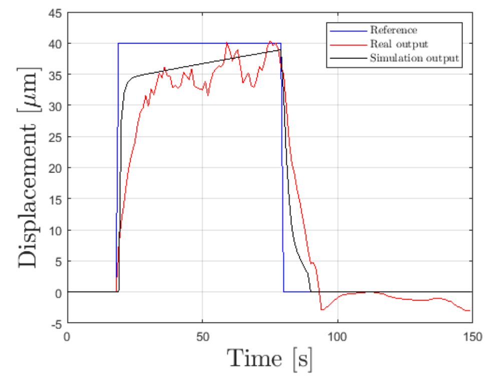

Fig. 11: Simulated displacement, real displacement, and reference.

sumption and the force produced with respect to the weight of the material has been compared with the performance of a DC linear motor (LINMOT PO1-23x80, `https://linmot.com/`) with comparable maximum output force.

From the technical data-sheet of the motor, it is possible to evaluate the consumption of electric power to produce the maximum amount of force. Referring to the experiment of Section V, the PU-based soft actuator, can produce a total maximum force F_{tot} given by:

$$F_{tot} = W \cdot g + F \tag{4}$$

where W is the weight of the free clamp expressed in N, g the acceleration of gravity, F is the contraction force of the specimen. The weight of the free clamp converted in N is comparable to the applied preload in the electromechanical characterization of Section III. This way, it is possible to reasonably use as reference the contraction force values obtained during the electromechanical characterization. The dissipated electric power P_{el} of the soft actuator is:

$$P_{el} = VI \tag{5}$$

where V is the applied voltage and I the current in the specimen.

For the comparison, it is assumed to realize an actuator with multiple bundles in parallel. The bundles contract in the same direction with the same force, and the electric current flowing in the specimen is the same for every bundle. It is possible to calculate the amount of total weight W_{tot} of the PU, which is required to produce the same amount of force generated by the linear motor with a simple proportion, knowing the force produced by the single bundle (F_{tot}) expressed in kg, its weight, and the force generated by the motor expressed in kg. If the bundles are connected in parallel, it is possible to calculate the number n of bundles necessary to produce the force generated by the motor, i.e.:

$$n = \frac{W_{tot}}{W_{bundle}} \tag{6}$$

where W_{bundle} is the weight of the single bundle. The total power consumption is given by:

$$P_{tot} = nP_{el} \tag{7}$$

The comparison of the energy analysis is summarized in Table II. The values of the current, relative to the bundle, used for the analysis have been measured with the high-voltage amplifier, and are referred to the maximum applied voltage of the test of Section V (i.e., 250 V), that leaded to a peak current value of 1.8 mA.

TABLE II: Comparison of the performances of a DC linear motor, a single bundle, and a parallel connection of several bundles.

	Weight (g)	Absorbed Power (W)	Max Force (kg)
Motor	265	280	4.486
Bundle	≈ 0.007	≈ 0.45	≈ 0.0234
Parallel bundles	≈ 1.34	≈ 86	≈ 4.486

VI. Robotic Arm

This Section presents the utilization of the PU-based soft actuator in a robotic system. Specifically, a specimen has been used to actuate a robotic arm to validate the contraction capabilities.

A 3D printed support has been realized, as shown in Figure 12. The bundle has been connected between the support and a rigid link, which is made of a conductive material and is free to rotate.

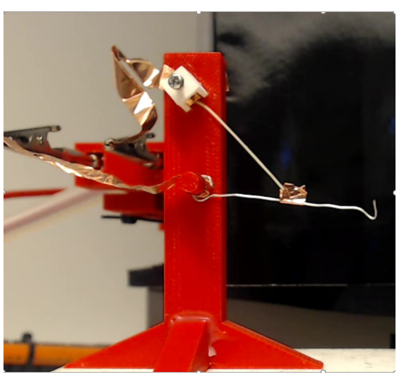

Fig. 12: The robotic arm actuated by the soft actuator.

After the preparation of the set-up, the specimen has been activated with a constant voltage of 300 V. The rotation of the robotic arm has been recorded with a camera and is plotted in Figure 13.

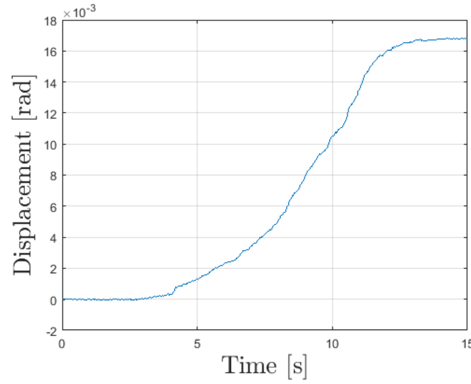

Fig. 13: Robotic arm rotation (in radians) when a constant voltage of 300 V is applied.

VII. Conclusion

In this work, a PU-based soft actuator has been analyzed. The actuator has been fabricated with an electrospinning process, with which aligned nanofibers of polyurethane and a salt have been produced. The soft actuator has been electromechanically characterized in terms of axial displacements and contraction forces, by using an Intron™Electropulse E1000 testing machine, equipped with a 5N load cell. A non-linear dynamic model of the soft actuator has been identified by means of an artificial neural network, which has been trained on the experimental data obtained during the electromechanical characterization. A PID-based position control has been designed on the identified non-linear model and tested on the soft actuator. Finally, a robotic arm, actuated with the PU-based soft actuator, validate the contraction capabilities of the actuator.

An energy analysis shows the performance of the soft actuator compared to a DC linear motor with comparable maximum output force. Specifically, the soft actuator is shown to be able to absorb less power and to have an overall weight two order of magnitude less than the DC linear motor.

Acknowledgments

The authors would like to thank Dr. Chiara Gualandi and Gianmaria Fornaia at the Department of Chemistry ”Giacomo Ciamician”, University of Bologna (Italy) for the fabrication of the PU-based bundle. and Carlo Gotti and Alberto Sensini, Department of Industrial Engineering, University of Bologna (Italy) for the support in the evaluation of the behavior of the PU- based bundle.

References

[1] J. Y. Cherng, T. Y. Hou, M. F. Shih, H. Talsma, and W. E. Hennink, “Polyurethane-based drug delivery systems,” *International Journal of Pharmaceutics*, vol. 450, pp. 145 – 162, 2013.

[2] Ohmukai, Masato, Kyokane, and Jun, “Electrode effects on polyurethane soft actuator,” *World Journal of Engineering and Technology*, vol. 05, pp. 520–525, 01 2017.

[3] H. Sakamoto, S. Amaya, Y. Sunahase, and S. ichiro Suye, “Fabrication and Characterization of FE/Polyurethane Nanofiber Actuator Prepared by Electrospinning,” *Journal of Fiber Science and Technology*, vol. 73, pp. 135 – 138, 2017.

[4] M. R. et al, “Electromechanical study of polyurethane films with-carbon black nanoparticles for MEMS actuators,” *J. Micromech. Microeng.*, vol. 24, 2014.
[5] D. Rus and M. T. Tolley, “Design, fabrication and control of soft robots,” *Nature*, vol. 521, p. 467 475, 2015.
[6] M. Thieffry, A. Kruszewski, O. G. T.-M. Guerra, and C. Duriez, “Dynamic control of soft robots,” *IFAC World Congress*, 2017.
[7] F. Largilliere, V. Verona, E. Coevoet, M. Sanz-Lopez, J. Dequidt, and C. Duriez, “Real-time Control of Soft-Robots using Asynchronous Finite Element Modeling,” *ICRA*, p. 6, 2015.
[8] S. Wittmeier, C. Alessandro, N. Bascarevic, K. Dalamagkidis, D. Devereux, and A. D. et al, “Toward anthropomimetic robotics: development, simulation, and control of a musculoskeletal torso,” *Artificial Life*, vol. 19, pp. 171–193, 2013.
[9] T. Calais and P. V. y Alvarado, “Advanced functional materials for soft robotics: tuning physicochemical properties beyond rigidity control,” *Multifunct. Mater*, vol. 2, 2019.
[10] R. O’Connor and G. B. McGuinness, “Electrospun nanofibre bundles and yarns for tissue engineering applications: A review,” *Proceedings of the Institution of Mechanical Engineers, Part H: Journal of Engineering in Medicine*, vol. 230, no. 11, pp. 987–998, 2016.
[11] N. Bhardwaj and S. C. Kundu, “Electrospinning: A fascinatingfiber fabrication technique,” *Elsevier,Biotechnology Advances*, vol. 450, pp. 325 – 347, 2010.
[12] H. Sjijberg, Q. Zhang, L. Ljung, A. Benveniste, B. Delyon, S. P.-Y. Glorennec, H. Hjalmarsson, and A. Juditskys, “Nonlinear Black-box Modeling in System Identification: a Unified Overview,” *Automatica, Elsevier*, vol. 31, pp. 1691 – 1724, 1995.
[13] O. Nelles, *Nonlinear System Identification, From Classical Approaches to Neural Networks and Fuzzy Models*. Springer, 2001, vol. 1.